Synthesis and Physical Properties of $Ba_xCu_{1-x}O$ (x =0, 0.2, 0.4) and $BaCuO_2$ Nanomaterials

AneeqaSafdar

Registration no. # 00000172976

A Thesis submitted in partial fulfillment of the requirements
for the degree of Master of Science

in

Chemistry

Supervised by: Dr. Zahida Malik

Department of Chemistry

School of Natural Sciences

National University of Sciences and Technology

H-12, Islamabad, Pakistan

2018

FORM TH-4

National University of Sciences & Technology

MS THESIS WORK

We hereby recommend that the dissertation prepared under our supervision by: ANEEQA SAFDAR, Regn No. 00000172976 Titled: Synthesis & Physical Properties of $Ba_xCu_{1-x}O$ (0<x>0.4) and $BaCuO_2$ Nanomaterials be accepted in partial fulfillment of the requirements for the award of **MS** degree.

Examination Committee Members

1. Name: DR. MUHAMMAD ARFAN   Signature: _____

2. Name: DR. REHAN ZAFAR PARACHA   Signature: _____

External Examiner: DR. NASIR MEHBOOB   Signature: _____

Co-Supervisor: DR. SHAH RUKH ABBAS   Signature: _____

Supervisor's Name DR. ZAHIDA MALIK   Signature: _____

_____
Head of Department

26/09/2018
Date

COUNTERSINGED

Date: 26/09/18

_____
Dean/Principal

THESIS ACCEPTANCE CERTIFICATE

Certified that final copy of MS thesis written by **Ms. Aneeqa Safdar**, (Registration No. **00000172976**), of **School of Natural Sciences** has been vetted by undersigned, found complete in all respects as per NUST statutes/regulations, is free of plagiarism, errors, and mistakes and is accepted as partial fulfillment for award of MS/M.Phil degree. It is further certified that necessary amendments as pointed out by GEC members and external examiner of the scholar have also been incorporated in the said thesis.

Signature: _____

Name of Supervisor: Dr. Zahida Malik___

Date: _____26/09/18_____

Signature (HoD): ____M. Arfan_____

Date: _____

Signature (Dean/Principal): _____

Date: _____26/09/18_____

Dedicated to

" My Father(Muhammad SafdarAwan),
Mother(AzraSafdar) and My Husband
(Muhammad AbidAwan)"

Acknowledgements

Abstract

Here we present the synthesis of Ba-doped-CuO and $BaCuO_2$ nanoparticles. Doped material was synthesized by hydrothermal method while $BaCuO_2$ was prepared by Citrate pyrolysis method. Characterization was accomplished by XRPD, SEM and EDS. Peaks of doped material and $BaCuO_2$ were also confirmed by phase analysis through XRPD analysis which confirmed the single phase synthesis of *Ba-doped CuO and BaCuO_2* with the crystallite sizes,30-53nm and 70nm, respectively. Samples morphology was studied by SEM and oboserved spherical morphology for undopedCuO and $BaCuO_2$, cubical morphology for $Ba_{0.2}Cu_{0.8}O$, and rod-like morphology for $Ba_{0.4}Cu_{0.6}O$. Absorbance was measured by using UV-Vis spectrophotometer. UV-Vis spectroscopy revealed band gab between 5.74eV for undopedCuO, the band gap for $Ba_{0.2}Cu_{0.8}O$ was greater than 6eV, and for $Ba_{0.4}Cu_{0.6}O$ was 5.8.eV while the band gap for $BaCuO_2$ was 5.77eV.From these results it was observed that least concentration of dopant gave the highest band gap. Dielectric loss, dielectric constant, ac conductivityand tan loss was evaluated. It was seen that the materials with least concentration of dopant shows best current storing ability as in case of $Ba_{0.2}Cu_{0.8}O$ values of dielectric constant, tan loss, ac conductivity and dielectric loss were 7×10^6, 10, 0.4 Sm^{-1}and7 $\times 10^7$, respectively. Physical properties of composites anticipate them good potential candidates for supercapacitor applications. TGA studies for thermal properties represented high stability of undoped and Ba doped materials without any phase change. And $BaCuO_2$ show slightly different behavior of absorbing oxygen from the environment. The total mass loss observed during TGA was about 4% to 12%.

.

List of Figures

List of Tables

Chapter 1: Introduction

Nanoscience

Nanoscience is a word comprises of two parts; "nano" and "science". The word "nano" has been derived from GREEK word "nanos" meaning "dawarf" and is a well-known as a prefix in nano-second, nano-ampere, and nanometer etc. with a mathematical representation of 10^{-9}. Whereas the word "science" covers a variety of fields likechemistry, biology, physics, electronics and superconductors etc. Hence it can be deduced that the study of any object in nanometer range is called nano-science.The concept of nanotechnology was announced by a physicist Richard Feynman in 1959 in his speak "*There's Plenty of Room at the Bottom*"[1]by definitionits "*The manipulation of matter on an atomic and molecular level*"[2].

Approachesfor the synthesis of nanomaterials

Nanomaterials can generally be prepared by two methods i) Top down approach, where macrostructures are milled or etched form bulk materials, and b) Bottom up approach where the nanomaterialsare synthesized by self-assembly and chemical synthesis method.The different methods for the synthesis of nanomaterial are summarized in Fig 1.1.
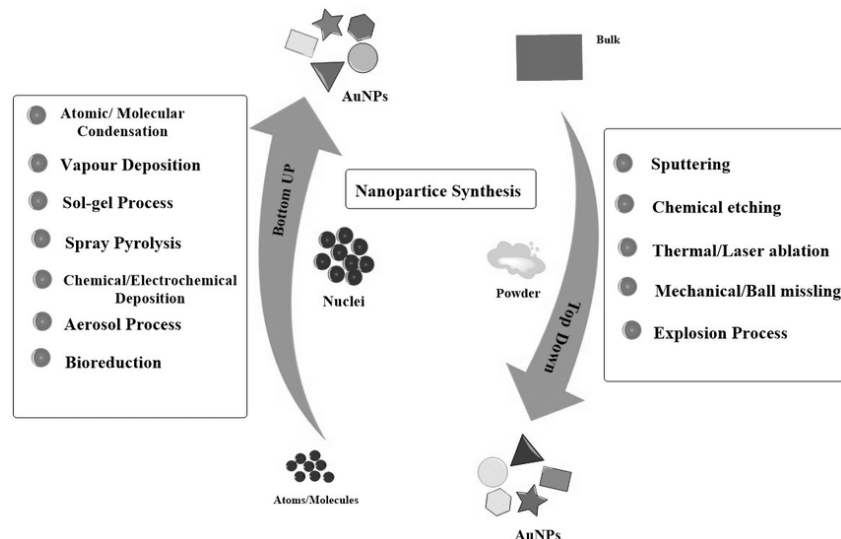
Figure 1.1. Methods used for the synthesis of nanomaterials

Nanoscience and nanotechnology are helping to improvemany technologies and industries.

Nanomaterial and their Classification
Nanomaterials have at least one dimension less than 100mn,mostly occur naturally e.g. lipoproteins, viruses and ferritin etc.On the basis of dimension, nanomaterials can be classified into three classes as shown in figure 1.2.

1.3.1.   0-Dimensional Materials.

The materials wherein all the dimensions are measured within the 100nm, e.g. nanoparticles, quantum dots, and nano shells are called 0-D materials. The movement of electron in 0-D material is confined in all three dimensions.

1.3.2.   1-Dimensional Materials.

Materials having at least one dimension out of the nanoscale range. This leads to needle like shaped nanomaterials with movement of electrons only in one dimension, e.g. nanotubes, nanorods and nanowires.

1.3.3.   2-Dimensional materials.

In 2D materials electron are confined only in one dimension while free to move in other two directions. 2-D materials exhibit plate-like shape. In this type of materials the electronic movement is confined only in one dimension and is allowed in remaining two dimensions, e.g. thin films, nanolayers and nano belts etc.

1.3.4.   3-Dimensional Materials.

The bulk materials that are composed of nanoparticles electrons are free to move in all dimensons and above 100 they have arbitrary dimensions. In these materials electrons are free to move in all dimensions and the movement of electrons is highly available because of their porosity. Certain types of nano structures and nano clusters are embedded in them due to which they show amazing properties[3, 4].
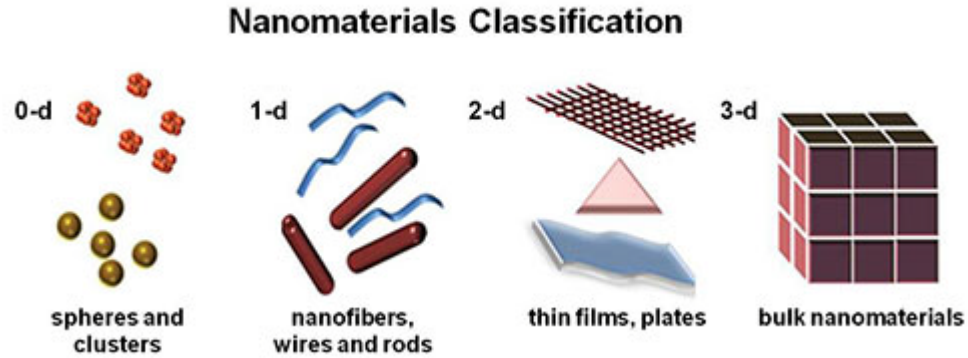
Figure 1.2. Classification of Nanomaterials

On basis of structural configuration.
The synthetic nanomaterials are again of six types. Based on structural configuration nanomaterials have four classes as discussed below.

- *a.* Carbon based nanomaterials: The main component of these materials is carbon. These materials could be ellipsoidal, hollow or tubes. For example; fullerenes are ellipsoidal, and nanotubes are cylindrical.

- *b.* Metal basednanomaterials: metal nanomaterials are are composed of metal particles like Au, Ag and metal oxides like TiO_2 and closely packed semiconductors like quantum dots.

- *c.* Dendrimers:Dendrimers are actually the polymers which are of nanometer size.On their surface there are so many chain ends which could be used for catalysis. They also have internal cavities in which new species could be carried and this property could be used for drug delivery.

- *d.* Composites:In composites different nanomaterials are combined to enhance their thermal, electrical, flame retardant and mechanical properties[5][6].

Properties of nanomaterials
Thenanomaterialsproperties are usually changed from their bulk complements and are highly reliant on upon their grain shape, size and atomic composition. Nano materials have the enhanced surface area and consequently high reactivity and the surface energy[7]. The unique properties of purposelymanufacturednanomaterials give them innovative capability in almost every field like medical, commercial, military and environmental sectors. Different properties of nanomaterials are explained below.

1.5.1.   Magnetic Properties

Magnetic nanoparticlesare used for in vitro diagnostics, drug delivery, MRI imaging therapeutic treatment, as contrast agents for, bio-separation, [8]. These nanoparticles are super-paramagnetic in nature, this propertyof nanomaterialsresulting from their petite size that is a few nanometers, a division of the width of a human hair (nanoparticles are about 1/1,000 reedier than human hair). Nanoparticles show Super-paramagnetic behaviorwhen external magnetic field is applied and become nan-magnetic in zero magnetic field. When returned to a zero magnetic field they quickly revert to a non-magnetized state. Super-paramagnatism is one of the most important properties of nanoparticles used for bio-magnetic separation.

1.5.2.   Optical properties

As the particle size reaches nano-scale the optical properties of materials get change from their bulk correspondent due to the following factors,

a.   Meager material effect
b.   Quantum confinement effect
c.   Surface plasmons
d.   Escalation of band energy
e.   Discrete band gap formed(quantized level)
f.   Formation of surface state

Nanomaterials show different optical properties then bulk because in nanoparticles electrons are not much free to move in any direction, because of their size.As electrons are not free to move in any direction so they behave differently at nano level. The optical properties the the materials also changes at naoscale level.i.e. gold show yellow in color at bulk level while atnanoscale gold look red in color.

1.5.3.   Mechanical properties

Mechanical properties of materialsalso show great difference at nano level like physical properties i.e.strength, melting point etc. also shows drastic change at nano scale level. For example at bulk level steel is very strong than carbon (graphite) but at nano-levelnanotubes of carbon are 100 times tougher than steel and show high flexibility.

1.5.4.   Electrical properties

Electrical conductivity increases with enhanced surface scattering and it reduces with limited dimensions. The electrical properties of nano-materials make them suitable for many technology applications [9]. Electrical properties are briefly described below.

Resistivity.The reluctance to the flow of electrical current is called resistivity. It is measured in Ωm and mathematical expression is given below

$$\rho = R\frac{A}{I}$$

Where l is the path length,Ris the *resistance,*andAis the *cross-sectional area* of the material. Now a day the target is to synthesize the materials with the fewer value of the resistivity for the establishment of low-cost electronics. Daniel Huang et al synthesized the low resistance gold nanoparticles [10].

Conductivity. The compatibility of a material for electrical current is called conductivity. Mathematically it can be expressed as follow,

$$\sigma = \frac{1}{\rho}$$

The gold nanoparticles show 70% enhanced conductivity as compared to the bulk [10]. The DC conductivity of NiO nanoparticles has been enhanced in order of six to eight times as compared to nickel oxide single crystal [11].

Dielectric strength. The capability of a material to tolerate the applied voltage expressed in kV/cm. It is inversely proportional to sample thickness, operating temperature and applied frequency. Nickel oxide nanocrystals with 2-3nm size show elevated values of ε' and ε'' at fewer applied frequencies because of viable dielectric amplification. All this can be credited to an existence of covering of conducting grain boundaries over the insulating grains [11, 12].

Temperature coefficient of resistance.Temperature coefficient of resistance is the variation of resistance with a change of temperature.and it is measured in per °C. The resistance increases with increase in temperature for the metals, e.g., temperature coefficient for silicon is -0.007 per °C.

Thermoelectricity.The materials which show thermoelectric effect are called thermoelectric materials. *Thermoelectricity* can be defined as the production of electric

voltage due to temperature difference and vice versa. The ability for thermoelectricity is measured by the figure of merit zT

$$zT = \frac{\propto^2 T}{\rho k}$$

Where $\propto$ is Seebeck coefficient, **ρ** is electrical conductivityand **k** is the thermal conductivity. The thermoelectric materials can be n-typeand p-type. For example, Al-doped ZnO (Al0.02Zn0.98O) is an n-type thermoelectric material with zT=0.3 at 1000K [13].

1.5.5.   Dielectric Properties

Doping of a material by another material changes its dielectric properties, because their dielectric response is different from that of individual components and varies with the amount of dopant material. Materials having low dielectric loss, high dielectric constant, high breakdown strength and ease of processing are considered as ideal material. Polymers show the mentioned characteristics but their dielectric constant is very low (2-5). On the other hand some materials have high dielectric constant but their dielectric loss is also high which limits their application e.g. $BaTiO_3$ has dielectric constant value in hundreds to thousands range but its high loss value reduces its applications. Therefore, to harness the advantages of polymers and ceramics, high *k* materials have been developed using various techniques one of which is core-shell strategy. High *k* materials have been used in energy storage devices such as capacitors. Solid $CaCu_3Ti_4O_{12}$ (CCTO) ceramics have been developed as a supercapacitor due to high dielectric constant (104 - 105 at room temperature) which is stable over a wide range of temperature. Doping of materials that can enhance the boundary resistance is another important technique to reduce the dielectric loss. Semiconducting grains and insulating grain boundaries make a heterogeneous structure which leads to high dielectric values[14-16].

1.5.6.   Thermal Peroperteis

A possible control over thermal conductivity and thermal expansion (CTE), by regulating initial composition and reaction conditions lead to the multifunctional applications of doped materials. The CTE knowledge of material is a prerequisite while

calculating dimensional changes and internal stress buildup upon exposure to temperature gradient. Thermal conductivity strongly depends on the corresponding properties of matrix and reinforcement. CCCs have been reported to show high thermal conductivities (5 times that of Cu) and can be excellent for electronic packaging applications to dispel the heat generated by the device. Particulate composites, comprising of heat conducting fillers and polymer matrix, have been used for this purpose because in addition to high thermal conductivity, they preserve the electrical insulation ability of the composites. Recently nanoparticles (Cu nanoparticles and carbon nanotubes) have been added to increase the thermal conductivity of composites [17].

Applications of nanomaterials

Nanomaterial exhibit astounding properties and a number of applications in various fields of chemistry, electronics biology and physics etc. Nanotechnology has put great and advanced products in numerous engineering fields because of their distinctive and satisfyingproperties like chemical, physical, and mechanical properties.
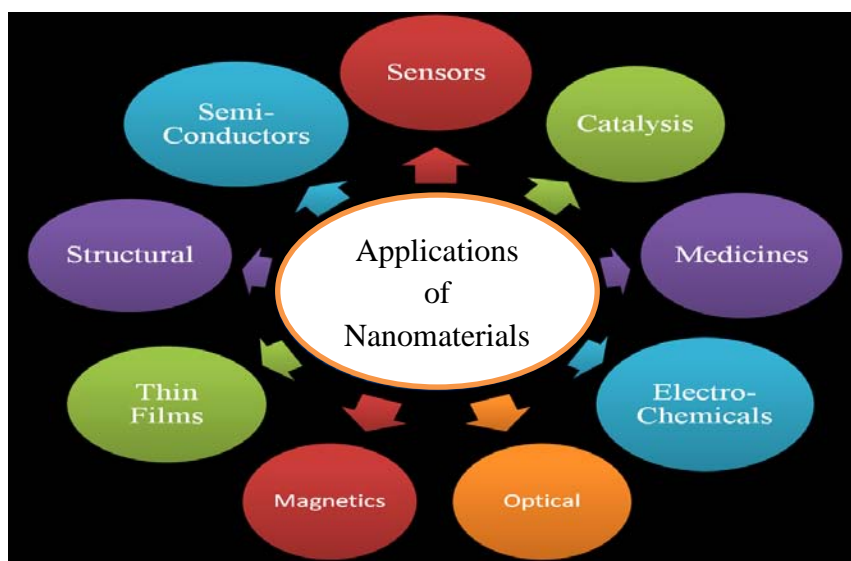
Figure 1.3.applications of nanomaterials

One of the property of nanomaterialsis that they have large surface area to volume ratio and this property make them suitableapplicant for wide range of fields. Large surface area to volume ratio and greater number of dangling bonds are required for the catalytic applications of nanomaterials in order to ensure their high reactivity.Many types of

nanomaterials like Au, NiO, and bimetallic Ni-Fe have been used in electro-oxidation of methanol, themal decomposition of ammonium perchlorate and hydrodechlorination of trichloroethylene to hydrocarbon respectively.Nanomaterials also show great involvement in bio-medicinal applocations, e.g. nano-biotechnology is used for tissue engineering for the purpose of scaffolding the injured and smashed tissues. They also exhibit promising properties in tissue repairing and regeneration. Nanotechnology has also been used to synthesis sensors to sense harmful pollutants and gases in air and environment e.g. CNTs, ZnOnanorods and SnO2nanowires.

Characterization techniques

1.7.1.   X-Ray Diffraction spectroscopy (XRPD)

It is a swift analytical method mainly used for limpidness and phase identification of a material. It provides information on unit cell dimensions, crystal system and crystallite size by measuring the intensities and angles of the beam diffracted by the sample.The basic principle behind XRPD is constructive interference between the crystalline sample and the monochromatic X-rays. The leading effect during this phenomenon is the scattering of X-rays which is known as diffraction. The diffraction of X-rays by the crystal has been elucidated by Bragg's law.

According to Bragg's Lawwhen an X-ray interacts with the crystal it is reflected from two points, surface of the substance and atomic planes inside the substance. The distance travelled by the X-ray, reflecting from the atomic planes depends upon the angle (θ) at which it enters the material and the separation between the atomic planes (d). For constructive interference the two reflected X-rays must have travelled an integral multiple of the wavelength (nλ). Mathematical Expression of Bragg's law is given below,

$$n\lambda = 2d\sin\theta$$

λ = Wavelength of incident light,

θ =diffraction angle

d =line spacing

as shown in figure 1.5.
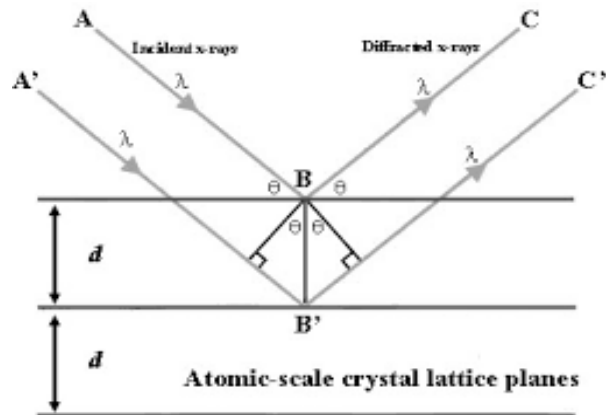
Fig1.4. Schematic diagram of XRD

Arrangement of atoms effect the intensity of diffracted waves, while the angle depends upon the shape and size of the unit cell of the substance. Most of the materials do not consist of single crystals rather they have polycrystalline powder with randomly oriented crystallites. The X-ray beam analyzes all the possible interatomic planes at different angles thereby detecting all the diffraction peaks.

1.7.1.4.   Instrumentation of X-Ray diffractrometer.
The three main components of diffractrometer are as following,

      a.   X-Ray tube or Cathode ray tube.

      b.   Sample holder.

      c.   Detector.

The filament in Cathode ray tube is heated to produce X-ray beam, consisting of electrons which are then accelerated by applied voltage and directed to the target area as a result characteristic X-rays are produced. The X-ray generated by target material(Mo, Cu, Fe, Cr) are collimated and oriented toward the sample. And finally detector record and processes the signals[18].

1.7.1.5.   Sample Preparation.
The steps for sample preparation are given below:

      a.   Few mgs of sample is taken.

      b.   Placement of sample onto the sample holder.
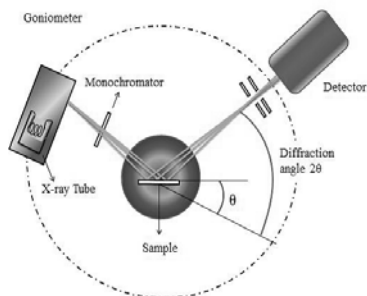
Figure 1.5. Instrumentation of XRD

1.7.1.6.   Uses and Applications of XRPD.

XRPD is a non-destructive technique which efficiently determines the crystal structure, crystallite size, phases present in the sample, atomic arrangement, lattice parameters and many other properties of the material. It is used in almost all the fields due to its versatility and accuracy in giving maximum structural information about the sample[19].

1.7.2.   Scanning Electron Microscopy(SEM)

"The scanning electron microscope was invented by Manfred von Ardenne in 1938."In SEM a beam of high energy electron is used to form a 3D image of the material under investigation with a resolution down to 1 nm. Itprovide information about, morphology, topography, compositional differences, phase distribution, and presences of electrical defects.

1.7.2.1.   Construction and working of SEM.

The main *components of SEM*are listed below:

      a. Electron gun.

      b. Electromagnetic lenses.

      c. Object chamber.

      d. Secondary electron detector.

      e. Display unit.

The electron gun consists of a tungsten filament which emits a stream of monochromatic electrons upon heating which are focused by the electromagnetic lenses. A beam is produced by condenser lens which condense the electron and also bounds the extent of current which regulates the diameter of the beam. While the electrons are focused by the second lense into a coherent, thin beam and high angle electrons are eliminated from it

by an objective aperture. The beam is scanned in a grid fashion by scan coil and finally the beam is focused on the sample by objective lens. The conducting sample is placed on the sample holder which can be inserted into the high vacuum chamber. The holder can be moved along X and Y directions.In addition it can be tilted, rotated and moved in Z direction for better resolution and specific area analysis. At the rear of the sample holder, secondary electron detector is located. The velocity and angle of the secondary electrons is related to the surface structure of the material. When these electrons reach the detector, an electronic signal is produced that is amplified and transformed into a digital signal observed on the display unit for further processing[20].
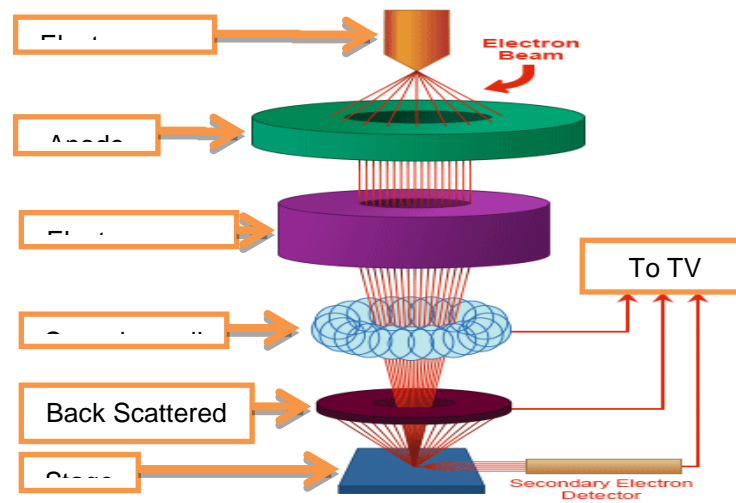
Figure 1.6. Schematic Illustration of SEM

1.7.2.2. Principal.

The interaction of electron beam with the sample results in the emission of various signals which include

1. Back scattered electrons (BSE).
2. Secondary electrons (SE).
3. Auger electrons (AE).
4. Characteristic X-rays.

All these signals yield different information about the sample under investigation. BSE and SE are commonly used for imaging. SE are important for evaluating the morphology and topography on samples while BSE are important for phase

discrimination and are more sensitive to heavier elements than SE. and they can detect image up to 10 to 15 nm. AE are specifically used for surface analysis in auger electronspectroscopy while the characteristic X-rays are used in EDX for sample's elemental and compositional analysis. [21].
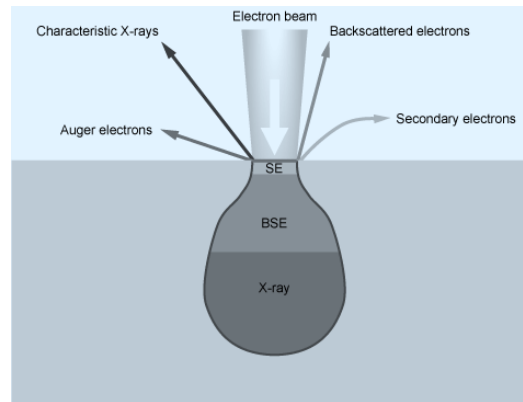
Figure 1.7. Different types of radiations emitted from SEM

1.7.2.3.   Applications of SEM

SEM is a non-destructive technique, so the same material can be analyzed repeatedly. It can be used in almost all the fields for observing structures up to 1 nm, mainly used for the topographic details of the object. BSE produced in SEM are used for phase discrimination of sample. SEM equipped with EDS can be used to find the elemental composition of the sample along with electron mapping at specific points.

1.7.3.   Energy Dispersive X-ray Spectroscopy

EDXis based on the principle that atomic structure of each element is unique in its own. That permit x-rays to identify the atomic structure of that element.It is most commonly tool chemical analysis tool in failure analysis. It is mostly used as an attachment to SEM. In EDS analysis can be performed within minutes and spectra can easily be interpreted. Its spatial resolution is very good[22].

When an incident beam is allowed to fall on a sample it excites inner shall electrons, which creates a hole after ejection. As a result to fill the vacancy an outer shell electron falls into the inner shell. X-rays are emitted as a result of energy alteration between the higher and lower shell. An instrument, energy dispersive spectrometer, is used to quantify the energy and number of the X-rays,discharged from the sample. As X-rays

have specific energy an element so it allows the measurement of elemental composition of a specimen.

1.7.4.   UV-Visible Spectroscopy

Band gap of a material can be studied by two spectroscopic methods:UV-visible spectroscopy and 2- DRS. UV-visible spectroscopy uses lights in visible and adjacent ranges. Atoms and molecules endure electronic transitionsin this region of the electromagnetic spectrum,. DRS is use to obtain molecular spectroscopic data. It is an optical phenomenon commonly used in UV-visible and infrared (near IR; NIR, mid IR; DRIFTS) regions. Powdered samples are usually used to obtain spectra and it requires small amount of sample preparation. When electromagnetic radiations are reflected from the surface a reflectance spectrum is obtained, which is collected as a function of frequency (wavenumbers cm^{-1}) or wavelength (nm).

After the interaction of the radiation with the sample, a combination of reflection, diffraction, refraction and absorption of incident radiation takes place (figure 1.13) [23].
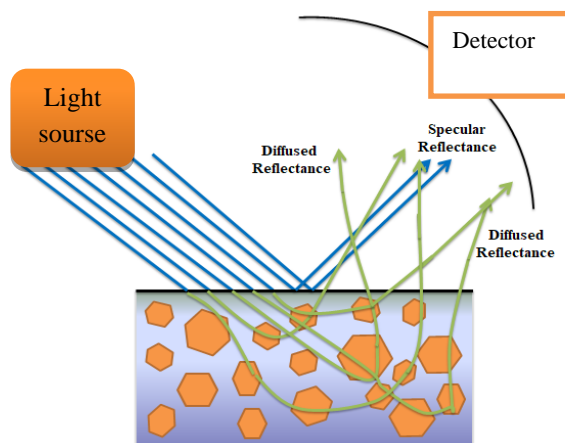
Figure 1.8. Pictorial Representation of UV-DRS Principle

Where F(R) is the

Kulbelka-Munk function, and R is the reflectance. The band gap of the material can be obtained by multiplying the coefficient with the energy (eV)

$$E_G = [F(R) \times h\nu]^n$$

Where exponent *n* is 0.5 in case of indirect bandgap transitions and 2 in case of direct band gap transitions [24].

Tauc Plot

In UV-DRS the graph is plotted against percentage reflectance and wavelength.100 % R implies that sample reflect 100% of UV wavelengths of light that interact with it. Graph between energy and $Eg(F(R))^2$ is also plotted. E_g is calculated by KubelkaMunk equation:

$$F(R) = (1-R)\ 2/2R = K/S$$
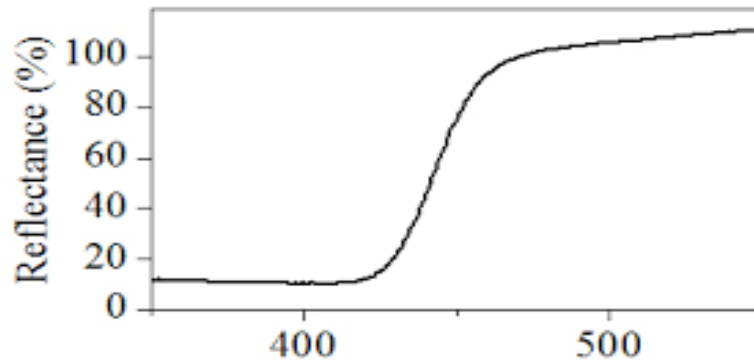
Figure 1.9 General Reflection Spectra

1.7.4.1.   Factors affecting the reflectance

Following are some factors which affect the reflectance are:

- Particle size:Smaller particle size gives improved spectra.Size should be 50 µm or less.
- Refractive index. The spectra of vastly reflected constituents will be more slanted due to specular reflectance constituent. This upshot could be abridged by sample attenuation.
- Homogeneity: Sample for diffusivity measurement should homogenous and well assorted otherwise sample is difficult to quantify.
- Packing. The sample should be loosely and evenly packed with min depth of 1.5 mm.

1.7.4.2.   Uses and Applications of UV-Visible

It is primarily used to calculate the band gap of materials. It is utilized in quality control of products in factories and is a refined tool for characterizing catalytic surfaces. The efficacy of solar cells can be resolute by quantifying the amount of reflected light flux.

Physical Properties

1.8.1.   Dielectric properties

Dielectric properties of materials can be studied by using LCR meter.LCR meter is named so because it can measure **Inductance (L), Capacitance (C) and Resistance (R)** of electronic devices.

1.8.1.1   Construction and Working of LCR meter

There are two common techniques used for LCR meters;

Wheatstone bridge method

The bridge method can be employed for measuring lower frequencies up to 100 kHz. A balanced bridge is used in this method so that at the balance point, the bridge constituents can define the assessment of constituent under observation. Commonly DUT is configured by wheatstone bridge and the DUT is positioned in a bridge circuit (figure 1.16). The impedance of DUT is denoted by Z_U in the circuit while the impedance of Z_1 is variable until no current flows through Z_U whereas, the impedances of Z_2 and Z_4 are well-known. The oscillator circuit works at frequencies that can be selected before the test and it normally lowers down up to 100 kHz. This is the balance spot of the bridge i.e. all four impedances obey following equation

$$\frac{Z_U}{Z_1} = \frac{Z_3}{Z_2}$$

Hence the impedance of DUT can be determined by using equation

$$Z_U = \frac{Z_3}{Z_2} Z_1$$
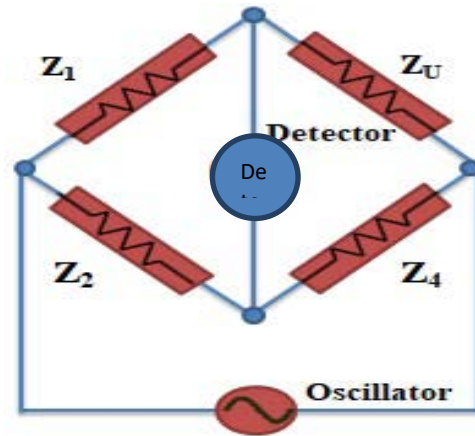
Figure 1.10 Circuit Diagram for Wheatstone Bridge

Current voltage measurement

For high frequency solicitations current-voltage measurementsare used. It is a precise measurement technology which can be operated at wide range of frequencies. In this technique, the current and voltage are measured for which two types of voltmeter and ammeter arrangements are used; one is for low impedance while the other is for high impedance. These measurements are made by a phase sensitive detector and the relative phase of current and voltage can be used to find out the impedance of DUT in terms of inductance, capacitance and resistance. These values are separately displayed on the screen. Sometimes, a transformer is used to isolate and enable these measurement but it limits the frequency range over which the measurements are made [25, 26].

1.8.1.2.   Uses and Applications of LCR meter

LCR meter is used for fault finding in electrical devices. It can be used to find quality factor, dissipation factor, tan loss (tanδ), and dielectric properties of the material.

1.8.2. Thermogravimetric Analysis

Thermogravimetry is an oldest thermal analytical technique and is still in use for studying the thermal behavior of materials. In TGA) deviations in weight of a sample can be measured as a function of time and temperature. A small amount of desired sample is required for analysis and the results are obtained in the form of a TG curve

with steps, depressions or hills at certain areas, describing the mass variation with temperature.

1.8.2.1.   Construction and Working of TGA

A TG analyzerentails of a pan braced by a precision balance, furnace programmed for a linear change in temperature with respect to time and an inlet for gases. The sample pans used in TGA depends upon the temperature conditions; commonly used pans include alumina crucible or platinum pans. TGA requires very small amount of sample (in mg) heated or cooled at desired rates during the experiment. The experiment can be carried out in air, inert gases (N_2, He, Ar), CO_2 or O_2 atmosphere depending upon reaction conditions. The corpus of sample is repeatedly monitored during the experiment a loss in it indicates degradation of the sample or removal gases and moisture from the sample which appears as a step in the TG curve and if the mass is increased, it is attributed to oxidation or reaction with the surrounding substances if any indicated by a hill in the curve. Figure 1.17 illustrates instrumentation of a simple TG [27].
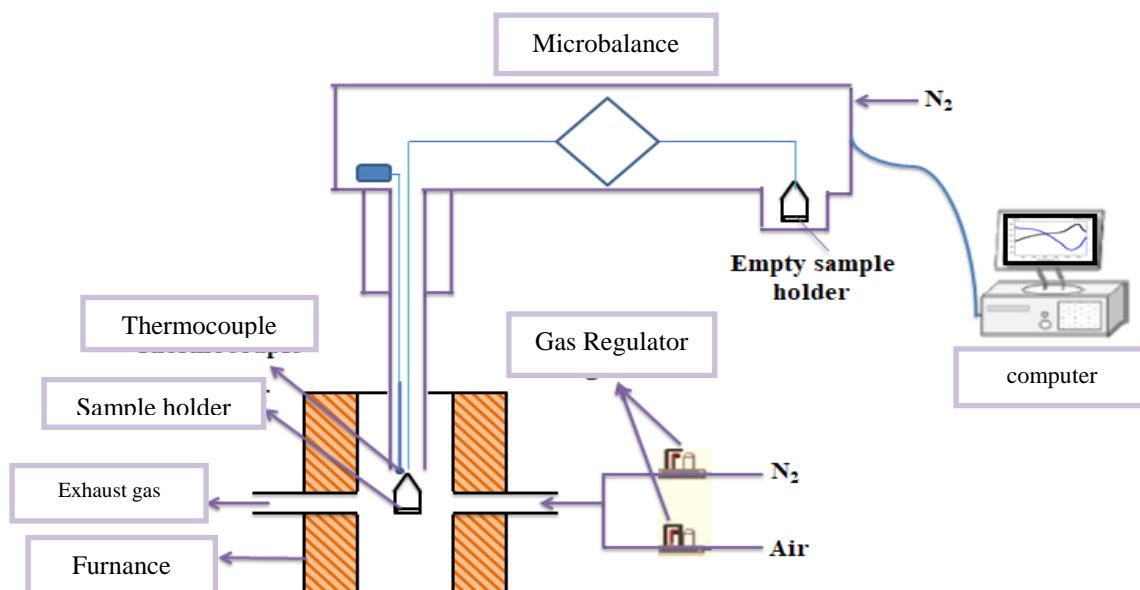
Figure 1.11. Instrumentation of a Simple TG

1.8.2.2.   Uses and Applications of TGA

TGA has wide applications in determining the thermal behavior, thermal stability and quality of the material. The purity of the sample, gas adsorption and desorption can be observed by this technique.

Chapter 2:Literature Review

Synthesis of inorganic materials especially oxides, carbonates and their compounds and doping of Barium and other earth alkali metals into TMO have gained importance due to their thermal, magnetic, electrical, mechanical, optical and industrial applications. Earth alkali metal oxides and TMOs will form compounds ABO_2, ABO_3 where the transition metal ion is smaller in size while earth alkali ion is large. In general practice precursors for the synthesis of doped materials and of perovskites i.e. ABO_2, ABO_3 includes , $BaCO_3$ and TMO which may be obtained by the reaction of required metal salts or can be used as such in the high purity form obtained from the dealers i.e. Sigma Aldrich, Deajung etc. Different methods of synthesis of doped materials and of Barium-Transition-Metal-Oxides, their precursors, properties and applications have been discussed in this chapter.

2.1. Precursors

Precursors which are generally involved in the synthesis of Earth Alkali doped TMO and of ABO_2, ABO_3 are, $BaCO_3$ and TMO are described in the following sections.

2.1.1. Barium Carbonate

$BaCO_3$ has three polymorphic forms namely orthorhombic, hexagonal and cubic. The orthorhombic phase, also known as Witherite, is the only stable form at ambient conditions. The name Witherite was given in honor of William Withering who was the first to recognize it in 1784 as a chemically distinct mineral from barites ($BaSO_4$) [28]. It undergoes transformation to hexagonal phase first (~1079 K) and then to cubic phase (~1237 K) upon thermal analysis [29]. In 2006, metastable monoclinic $BaCO_3$ was synthesized by rapid quenching during the flame spray pyrolysis method, it was reported that the monoclinic phase gets transformed to stable orthorhombic phase after few days at room temperature [30].

2.1.2. Transition Metal Oxides

Transition metal oxides are composed of oxygen atoms attached to transition metals. They are generallyconsumed for their semi-conductive and catalytic properties. TMOs are also commonly used as pigments in plastics and paint industry, particularlyTiO_2.

Transition metal oxideis a class of materials with fascinating properties like, chemical mechanical and electronic properties. They retain tunable electronic and photon conveyance properties and also stable at high temperature. In general they have high thermoelectric properties.[31].

2.2. Synthesis

2.2.1. Doping of Earth Alkali Metals in TMO

2.2.1.1. Mg Doped Iron Oxide

William B and Shahed Khan in 2004 reported the synthesis of stable Mg-doped iron (III) oxide thin film electrodes by spray pyrolytic method. As synthesized Mg doped Fe_2O_3 showed p-type behavior. The sample of Mg-doped p-Fe_2O_3 prepared at optimal temperature of 390 °C at 0.2 V/SCE showed the highest photocurrent density of 0.22 mA/cm^2. For the Mg-doped p-Fe_2O_3 thin films, XRD results showed mixed structures (α and γ-Fe_2O_3 and MgO) [32]. In 2014 Reza Zamiri et al reported low cost wet chemical method for successfull synthesis of Mg doped ZnOnano-plates. XRD, SEM, EDS and UV-Vis spectroscopy techniques were used for material analysis. XRD used for phase identification and crystallite size was about 30.3mn measured from XRD data. SEM for morphological analysis, EDS for elemental composition and UV-Vis spectroscopy for determining the band gap were used. They reported that band gap was decreasedby Mg doping. They also reported that These Mg-doped ZnOnanomaterials showed great applications in the optoelectronic devices[33].

2.2.1.2. Ba doped TiO$_2$

Jae Ek Son et al in 2009 reported the synthesis of Ba doped TiO$_2$catalyst with hollow sphere morphology, with various compositions. In acidic media they evaluated their electrocatalytic activity. TiO$_2$ hollow sphere were synthesized by using poly (styrene–methacrylicacid) latex as template, and BaCl$_2$ was used precursor during barium doping above spheres. BET, XRD, TGA and SEM analysis were usedfor characterization of Ba/TiO$_2$ hollow sphere. XRD confirmed BaTiO$_3$ and rutile TiO$_2$ phases in the catalysts. TEM results showed the formation of hollow sphere formation with even layer of barium arround the spheres. rRgardless of the deviation in calcination temperatures 0.4–

0.5 mm diameter of Ba-doped TiO_2 hollow sphere was found. iI acidic solution Barium doped titania hollow spheres showd long time electrocatalyticpermanency[34]. In 2016 K. Vijayalakshmi and D. Sivarajreported the microwave assisted method for the synthesis of TiO_2 and Ba doped TiO_2. They reported the use of these materials in antibacterial activity. XRD, SEM,EDX FTIR and UV-vis spectroscopic techniques were used to characterized the material.. XRD results showedthat, after Ba^{2+}doping, differently oriented (101) TiO_2anatase phase, was changed to anatase–rutile mixed phase. With Ba addition in TiO_2, a significant shift was observed in vibrational spectra show significant shifts in the peaks. The optical spectra discoveredincreased band gap with Ba doping, thereby permitting the deferral in recombination rate, supporting antibacterial activity. After Ba doping, the surface morphology with sphere-shaped grains with amplified porosity of TiO_2 was observed. Phase purity of prepared material was confirmed by EDS analysis. Ba doped TiO_2 exhibited greater antibacterial activity than pure TiO_2 nanoparticles[35].

2.2.1.3. Ba doped ZnO

In 2014 GunjanSrinet et al reported thermal decomposition methodology for the production of Ba-doped-ZnO. They deliberated the consequences of Ba doping on structural, optical and ferroelectric properties of ZnO NPs. ZnOrevealed Wurtzite structure in XRD results which confirmed that replacement of Ba on Zn sites have occurred. SEM was used for morphological identification. In UV-Vis spectra redshift in band gap was observed as a result of Ba-dopingwhich was buoyed by PL spectra which showed that defects states have been increased by Ba doping. High value of transition temperature at (~330°C) and large value of dielectric constant were observed in dielectric studies[36]. In 2015 KekeliN'Konou et al successfully synthesized Ba-doped-ZnO NPs by microwave hydrothermal methodology. They explored the consequences of Ba-doping on optical and physical properties of ZnO NPs. XRD analysis exposed that ZnO NPs were polycrystalline. The diameter crystallite size found to fluctuated from 20 to 21.5 nm. SEM analysis was done of surface morphology and reported that the sample was influenced by Ba impurities[37]. In 2016 Reza Zamiri et al used precipitation process for Ba doping inZnO and investigated their optical properties. XRD was used to determine the lattice parameters like lattice strain and crystallite size by Williamson Hall

method. This method reported that average crystallite size was increased by Ba doping. The temperature dependence of PL emission reported that at lower temp the sample showed sturdier emission than at room temp.in both UV and visible region[38]. In the same year KekeliN'Konou et al studied the effect of Ba-doping on structural, optical and morphological applications of ZnO NPs. They reportedsonochemical process for the synthesis of Ba-doped-ZnO nanoparticles. The FTIR and XRD results showed that ZnO NPs were polycrystalline with customary hexagonal wurtzite crystal structure. SEM was used for morphological analysis. And elemental analysiswas done by EDX which confirmed the incorporation of Ba. [39]. In 2017 BehnazShirdel and Mohammad A. Behnajady synthesized Ba doped ZnO by a facetious sol-gel method without using surfactant. They investigated the effect of calcination temperature and Ba-doping on the performance of Ba/ZnO NPs. They stated that extremephotocatalytic activity was attained by 0.1% dopping of Ba inZnO NPs at 400°C annealing temperature. XRD, EDS, TEM, SEM,DRS and nitrogen physisorption methods were employed for determining the properties and structure of Ba/ZnO NPs. XRD results did not exhibit any peak concerning to Ba in Ba/ZnO NPs. SEM analysis determine the spherical morphology for Ba/ZnO nanoparticles. DRS patternshowedthat by Ba doping a reduction in band-gap energy can be observed as comparedtopureZnO**[40]**.

2.2.2. Synthesis of Barium Transition Metal Oxides

2.2.2.1. Barium Scandate

The hydration performance of the barium scandateswas studied in 2006 by TakahisaOmata, in comparison with oxygen-deficient perovskite-related structures of tetragonal $Ba_2Sc_2O_5$ and cubic $BaScO_{3-\delta}$. Two methods were followed for the synthesis of polycrystalline samples ($Ba_2Sc_2O_5$). One was the solid-state reaction of two precursors i.e. barium and scandium oxalates, The other was the thermal decomposition of the complex hydroxide. XRD patterns of the samples synthesizedvia the solid-state reaction between barium and scandium oxalate exhibited that the acquired sample was having a trace of Sc_2O_3. While the XRD results of the sample acquired by the putrefaction of $Ba_3Sc_2(OH)_{12}$ at 1073 K for 20 h in air exhibited that the diffraction lines were indexed as those for a cubic perovskite structure[41].

2.2.2.2. Barium Titanate

In 1989 expeiments were performed by A Beaguretal to obtained the desired metatitanate $BaTiO_3$. They discussed the part of reaction conditions and effect of transformation time and i.e. in air existence of $BaTiO_3$ was in rivalry with that of orthotitanate Ba_2TiO_4. And presence of Ba_2TiO_4troubles the electrical properties of high dielectric constant ceramic of which $BaTiO_3$ was the chief component[42]. In 1997 S. Urek& M. Drofenik hydrothermally synthesizedfine powder of $BaTiO_3$. $BaTiO_3$ powder, displayed $BaCO_3$ impurities synthesized from $Ba(OH)_2$. while, powders synthesized from $Ba(CH_3COO)_2$, $Ti(OC_2H_5)_4$ and tetramethylammonium hydroxide did not show any malfunction and the smallest average grain size [43].Table 2.1 shows the outcome of precursors on the crystalline and grain size of the particles.

Table 2.1.effect of precursors on the crystalline and grain size of the particles

Sample code	Precursors	Crystallite size(nm)	Grain size(μm)
BT	$Ba(OH)_2$ and $Ti(OC_2H_5)_4$	20.8	3.5
BTA	$Ba(OH)_2$, $Ti(OC_2H_5)_4$ and NH_4OH	20.3	4.3
BTH	$Ba(OH)_2$, $Ti(OC_2H_5)_4$ and N_2H_5OH	19.0	3.3
BTT	$Ba(OH)_2$, $Ti(OC_2H_5)_4$ and $(CH_3)_4NOH$	20.7	4.5

In 2000 Xiuling Jiao and Dairong Chen from Shandong University of China synthesized single phase $BaTiO_3$and found that the synthesis of $BaTiO_3$ powders via solvo-thermal reaction was more challenging, in contrast to hydrothermal processing.Cubic $BaTiO_3$ powders were synthesized solvo-thermally[44]. In the same year Song Wei Lu et al tailored $BaTiO_3$nano crystals from polyoxyethylene(20) and sorbitanmomooleate (tweent 80),which were used as surface modifier, by hydrothermal at 230°C for 0.5 to 2 h. By TEM analysis the mean particle size they obtain was 77.8 ± 23.5nm and the particle size calculated with, laser scattering particle size analyzer, was 83 ± 19 nm. They reported that additionaldevelopment and accumulation of nanocrystals have been delayed by surface modifier as the size distribution was narrow. XRD and DSC identified these nanocrystals as metastable cubic phase BT. While Raman spectroscopy identified the tetragonal phase which was Raman active.[45]. IN 2005 L. Simon-

Seveyrat et al re-investigated $BaTiO_3$ synthesis via by predictable solid state reaction and oxalate co-precipitation process and the attained powder showed high piezoelectric and dielectric properties[46].

In 2007 Tomoaki KARAKI fabricated the lead free piezoelectric ceramics, Barium titanate ($BaTiO_3$.Thebiggest grain size was less than 3 mm and the average grain size was about 1.6 mm [47].

In 2010 Che-Yuan Chang et al reported modified solid-state method to synthesize submicron $BaTiO_3$ particles. $BaTiO_3$ powders were synthesized vianewproductionmethod. Submicrometric$BaCO_3$ NPs were coated over TiO_2 particles which were separated by urea disintegrationprocess. $BaTiO_3$nanoparticles were efficaciouslyacquired after heat curing at 1000 °C for 1 h. The size of the attained particle was arround 150–200 nm, which was in contract with the original size of the TiO_2 core[48].

S. Fuentes et al in 2010 introduced a novel synthetic method to synthesize higher limpidness barium titanate, ($BaTiO_3$). They synthesized $BaTiO_3$ via sol–gel-hydrothermal process from TiCl4 and BaCl2 solution which were used as starting materials, in an oxygen enviroment. By employing this method spherical nanoparticles of $BaTiO_3$ were obtained, with grain size of about 50nm at synthesis temperature of 200°C, which was determined by XRD. The composition and microstructure of as synthesize BaTiO3 nanoparticles was determined by XRD, HRTEM, AFM EDS and Raman spectroscopy[49]. In 2011 Sonia et al synthesized Barium titanate ferroelectric system,at lower temperature, by using powderresulting from modified solid state reaction (MSSR) and sintering was done via microwave (MW) processing method. [50].

In 2012 Yao-Feng Zhu et al synthesied the $BaTiO_3$ nanotubes by simple wet chemical method at lower temperature (50°C).Cubic phase was exhibited by $BaTiO_3$ nanotubes.Average diameter of these particles was about ~10 nm and wall thickness was about 3 nm[51].In 2015 Xia Zhao et al, employed solid state route for the synthesis of $BaTiO_3$ ceramic from fine powder.the average particle size of these materials was 400nm and witetragonality of this material was 1.0103[52].

2.2.2.3. Barium Vanadate

In 1993 Guo Liu and J.E.Greedan synthesized$BaVO_{2.8}$in a very hagh purity hydrogen gas, by reducing $Ba_2V_2O_7$at 1350°C[53]. In 1995 Yoshio Oka et al reported the hydrothermal synthesis of BaV_3O_8 from VO(OH)$_2$ and $BaCl_2$that resulted in the formation of black crystal rod like shape which exhibited the monoclinic system[54]. In 2008 ParveenKhatri et al synthesizedpolycrystalline sample of $Ba_3V_2O_8$ by solid state method at very high-temperature. That result in the production of single phase materialwith hexagonal crystal system[55]. In 2011 Jing Xureported composite hydroxide mediated for the synthesis of barium vanadate at 200°C, from V$_2$O$_5$ and BaCl$_2$for 13 h. Synthesized materials exhibited flower-shaped morphology [56]. In 2014 Kousuke Nishimura et al reportedhigh-pressure synthesis method for a new cubic perovskite$BaVO_3$[57].

2.2.2.4. Barium Chromate

In 1968 B. L. CHaMBERLAND prepared several hexagonal $BaCrO_3$ polytype at high temperature and high pressures in a tetrahedral anvil apparatus[58].In 1979 Paul S Haradem et al synthesized Twenty-seven-layer barium chromium oxide.$BaCrO_3$, was synthesized at 60-65 kbar and 1200°C by reaction of CrO_2 and Ba$_2$CrO$_4$[59]. Then again in 1982 and 1983 B. L. Chamberland synthesized the 4 and 6-layer hexagonal $BaCrO_3$ polytype, at high pressure and high temperature. $BaCrO_3$obtained in these method were hexagonal black crystals[60, 61]. In 2014 and 2015 Angel M. Arevalo-Lopez et al synthesized BaCrO$_3$with 6-layered hexagonal polymorph structure at 900-1100 °C under 9-22 GPa pressure. This hexagonal structure showed stability when cooling down to 5 K[62, 63].

2.2.2.5. Barium Manganite

In 2006 C.G.Hu et al reportedbarium manganite (BaMnO$_3$) nanorods/nanowires via size-manipulable synthesis of single-crystalline of by using the composite-hydroxide-mediated approach. This method synthesized hexagonal perovskite structure and which showed nanorods morphology with width ranging between 50-100nm[64].

2.2.2.6. BaFeO$_3$

In 2007 a photocatalyst BaFeO$_3$ was synthesized via citrate–nitrate combustion method by Yang Yang et al. and this photocatalyst was used for the photodegradation of methyl orange under UV light irradiation[65]. In 2011 Naoaki Hayashi et al prepared a new perovskite was prepared, BFO($BaFeO_3$) which showed a new cubic (Fe^{4+}). This perovskite was synthesized by low-temperature oxidation reaction using ozone.While any application of a verysmall external field encouraged ferromagnetism with a higher atomic moment of 3.5 mB per Fe^{4+} ion. BFO was thus the first reported iron oxide which showed ferromagnetism at ambient pressure[66].

2.2.2.7. BaCoO$_3$

In 2004 by V.G. Milt studied that BaCoO$_{3-\delta}$mixed oxide can be used for combustion of diesel soot and for the ofNOxas well. Nitrates of Ba and Co were used as starting materials and stoichiometric mixture was prepared[67]. In 2015 QiuwanShen et al synthesizedBaCoO$_{3-\delta}$ perovskite powders by using microwave-assisted EDTA technique[68].

2.2.2.8. BaNiO$_3$

In 1974 Yasuo Takeda et al reported that single crystal of BaNiO$_3$wereprepared under oxygen pressure of 2000 bars. And their unit cell was reported to be hexagonal[69]. In 2016 Jin Goo Lee et al synthesized BaNiO$_3$which showed hexagonal perovskite structure. Thickness of nanostructure was 100 μm. BaNiO$_3$ exhibited hexagonal rod shaped morphology.BaNiO$_3$wasmanufactured by flux mediated crystal evolution. [70].

2.2.2.9. BaCuO$_2$

In 1991 Ch. KRUGE et al reported that different methods were developed to optimize the synthesis of BaCuO$_2$. BaCuO$_2$was synthesized by wet chemical method.Co-precipitation method was followed for this synthesis. Oxalates or hydroxycarbonates were characterized and their reactivity was related with the conventional ceramic method. In which BaCO, and CuOwere used as starting material and firingof a mixture of theis precursors gave the product. DTA, XRD and IR-investigations were carried out to characterize these materials. This became imaginable because the disintegration of these precursors to BaCO, and CuO was finished up to 600 °C**.** thus, the same reaction

was monitored for the formation ofBaCuO$_2$[71]. In 1993 Wu Mingmei et al reported that the compound BaCuO$_{2.5}$was attainedby using BaO$_2$and CuO as starting material. This p-type semiconductor belongs to orthrombic system and paramagnetic in nature, following Curie's Law inthe measured temperature range from 77-220 K [72].

2.2.2.10. BaZnO$_2$

In 1959 U Spitsbergen investigated the system Ba-M-O, where M represented the Co, Ni, Mn, Zn and Be. In experimental section they weighed $BaCO_3$ and $M^{II}O, M^{III}CO_3$ in 1 ratio 1 (1:1) and ablazed in high vaccum or in a flow of a suitable gas in a resistance furnance at temperature upto 1100°C. by Weight loss confirmed the completion of the reaction [73]. In 2018 Yi-Chai Chiang, et al reported the fabrication and characterization of Ba-deficient **$BaZnO_2$** $(Ba_{1-x}ZnO_2)$ nanowires. They developed a flippantproduction method of $Ba_{1-x}ZnO_2$ by pH modulation using solvothermal synthesis[74].

2.3. Properties

2.3.1. Electrical properties

Electrical properties of Barium Scandate were studied in 2006 in dry and wet atmosphere respectively[41]. In 1989 JukichiHombo et al studied perovskites$SrFeO_{3-\delta}$ and $BaFeO_{3-\delta}$ and measured their conductivities and the Seebeck coefficients in air, O$_2$, and N$_2$. The temperature was ranged from 650°C to room temperature[75]. S. Fuentes et al in 2010, reported sol–gel-hydrothermal for the synthesis of BaTiO$_3$. TiCl$_4$ andBaCl$_2$ were used as precursors . and the reaction was carried out in an oxygen atmosphere. They obtained particles with grain size of 50nm[49].

1.3.5.   2.3.2. Dielectric properties

In 2005 L. Simon-Seveyrat et al presented that BaTiO$_3$ have piezoelectric d_{33} constant higher than 260 pC/N at about 25.8°C. This rate was higher than frequently reported ones for BaTiO$_3$ceramics: at room temperature the values of ε$_r$ (1kHz) and d_{33} were around 1700 and 190 pC/N respectively. The piezoelectric and electrical properties were also largely superior to the other perovskite lead-free materials[46]. In 2007 Tomoaki KARAKI et al fabricated the lead free piezoelectric ceramics.The values of dielectric

constant ϵ^T_{r33} of the poled model was 5000 and 42%. electromechanical coupling factor which was represented by k_p.[47].

In 2011 Sonia et al synthesized of microwave sintered $BaTiO_3$ ceramics and studied its dielectric, ferroelectric and piezoelectric properties. At room temperaturedielectric loss (tan δ) and dielectric constant (ϵ_r) were found to be ~2500 and 0.03 respectively. [50]. In 2015 Xia Zhao studiedthat $BaTiO_3$ ceramics show improved of ϵ_r 12,000 at Curie temperature of 125 ºC, and studied its properties[52].In 2008 ParveenKhatriand her co-workers calculateddielectric properties of $Ba_3V_2O_8$ and they studied dielectric properties of the compoundat different temperatures (25–400 °C),in wide range of frequency (102–106 Hz), found that these properties were temperature reliant. The electrical behavior of this material wasstrappingly dependent on temperature and frequency. The activation energy, in high temp region, was 0.23eV at 50 kHz[55].

2.3.3. Thermal properties

The impurity phases present in the high temperature superconductors largely effect the physical properties of ceramic high Tc. I Halasz et al in 1988 investigated $Ba_2Cu_3O_{5+d}$, synthesized at different temperature, by TG-DTA connected with XRD. They reported that at lower temperature tetragonal phase with large oxygen content appeared[76].In the $YBa_2Cu_3O_{7-y}$ system (YBaCuO)scums with varied phases of $BaCuO_{2+x}$(BaCuO) were of prodigioussignificance. T. KOPTE and E. HEGENBARTH studied these properties of BaCuO in 1989[77]. In 1993 A.F.Miorova et al reported thermal analysis (TG-DSC) of $Ba_2Cu_3O_{5+\delta}$(023), which was a pure compound, at 25–970°C temp range and oxygen pressures of 0.21 and 1 atm. They investigated that the compound (023) disintegrated at a temperature of 758°C at 0.21 atm oxygen pressure and in 1 atm O_2 it disintegrated at 806°C.[78]. In 2009 NehaTopnani et al synthesized the CuOnanopowder by wet synthesis method. They performed various characterization techniques to study the material i.e. XRD, SEM-EDS, TEM ,FT-IR, BET UV-Vis, TGA/DSC. To have an idea about the crystallinity temp TGA was performed. In both nanomaterials (Cu_2O and CuO), the first mass loss was attributed to the removal of H_2Oat about 150◦C and were represented by endothermic peaks in DTA curve. At 850◦C second mass loss occurred that can be credited to the removal of organic moieties. No more mass loss was observed at high temperatures, thus supporting the crystallinity with high purity[79].

2.3.3. Microwave absorption properties

In 2012 Yao-Feng et al synthesized the $BaTiO_3$ nanotubes. Theystudied microwave absorption properties nanotubes of $BaTiO_3$ at microwave frequencies ranging from 0.5 to 15 GHz. The minimum reflection loss of the $BaTiO_3$ nanotubeswas, at 15 GHz, that was extended to 21.8 dB. The outstanding absorption capability of $BaTiO_3$ nanotubes at very high frequency designated that these nanomaterials could be proved as auspicious microwave-absorbing materials[51].

2.3.4. Magnetic Properties

In 2011 Jing Xu synthesized$BaVO_3$ with flower-shaped morphologyand studied that the ferromagnetic performance of $BaVO_3$nanoflowerswas due to the coercivity of 18.89 Oemagnetization of about 83.50× 10^{-3} emu/g, and remnant magnetization of 4.63× 10^{-3} emu/g, which was chiefly due to the occurrence of a non-orthovanadate phase with S = ½ spin [56]. In 2014 Kousuke Nishimura et al reported$BaVO_3$ for the first time[57]. While its magnetic properties were studied by V.V. Bannikov in 2015[80]. In 2014 Angel M. Arevalo-Lopez et al synthesized$BaCrO_3$ with 6-layered hexagonal polymorph structure. They observed that, below Curie temperature TC = 192 K, ferrimagnetism with a very small saturated magnetization of approx. 0.1 µB[62]. In 2011 Naoaki Hayashi et al studied magnetic properties of $BaFeO_3$ and found that ferromagnetism could be induced due to the presence of a very small external field which was about 3.5 µB per Fe ion[66]. In 1974 Yasuo Takeda et al reported $BaNiO_3$ and found that magnetic susceptibility of $BaNiO_3$ was nearly temperature independent down to 4.2 K, showing diamagnetic behavior of$BaNiO_3$[69].

2.4. Application Of Barium-Transition metal-oxides

Several applications of Ba-TMO have been studied. The most commonly studied applications arethat the $BaTiO_3$was an important ferroelectric material with wide range of utilization in resistors, transducers, piezoelectric devices and semiconductors. It exists in five altered crystallographic forms as1-cubic, 2- orthorhombic, 3-hexagonal,4-rhombohedral, and 5-tetragonal. The two forms i.e. cubic and hexagonalwere paraelectric (temporary polarization) on the other hand orthorhombic,rhombohedraland tetragonal were ferroelectric in nature. The strongly basic nature of $BaCO_3$ modifies

titania and improves its dye sensitized performance in solar cells. It basically changes the direction of conduction band of TiO_2 toward negative direction ultimately increasing its conversion efficiency. Doping is important for attaining required characteristics for certain applications and the perovskite structure of $BaTiO_3$ makes it easier to incorporate ions of different sizes thereby allowing variety of dopants to be easily accommodate e.g. ZrO_2 doping improved the dielectric properties of $BaTiO_3$[81-87].

Barium Ferrites is another important material synthesized via mechanical alloying in which grain size is important in determining the magnetic properties. $BaCO_3$ enhances the magnetization of nano-ferrites which makes them useful for hard magnetic applications. It induces phase transformation which modifies the structure and also transforms the magnetic response (ferromagnetism). This method is useful for synthesizing eternal barium hexaferrites which are appropriate for magnetoelectric devices. By carefully controlling the dielectric properties Barium Ferrites can be used as supercapacitors and in microwave applications.Apart from these, they are also used in barcode and recording devices [88-91].

Barium Niobate ($BaNbO_3$), synthesized via composite hydroxide mediated method using $BaCO_3$ and Nb_2O_5, has been found to be an excellent candidate for humidity sensing electronic devices. It acts as a superconductor at 18.6 K and has been used as a precursor for the synthesis of $Sr_xBa_{1-x}Nb_2O_6$perovskites($0.25 <x< 0.75$) which is a ferroelectric ceramic material. $BaNbO_3$ possess higher anticorrosion performance and higher stability, and is also used in chemical and nonvolatile memories, capacitors,chemical sensors,and multilayer ceramic[92-97].Barium Zirconate ($BaZrO_3$), like other Barium composites, exhibits perovskite structure and is of great importance in high temperature applications. It is thermally stable and does not undergo phase transition from 1327 °C down to -269 °C which makes its suitable for thermal barrier coating applications. It is also used as a container for growing crystals of high Tc like YBCO because of its chemical inertness with them[98, 99]. Along with $BaZrO_3$, Barium Cerate ($BaCeO_3$) is used for better protonic conduction. $BaCeO_3$ is unstable in CO_2 atmosphere so $BaZrO_3$ is added to improve its stability. Due to high temperature ionic conduction, it is used in hydrogen gas sensors, and hydrogen production[100, 101]. $BaCO_3$ and CuO have been

used for the synthesis of $BaCuO_x$ based high Tc namely commonly known as YBCO. It was found that in synthesizing YBCO, CuO acts as a catalytic agent for the decarbonation of $BaCO_3$ and results in the formation of $BaCuO_2$. The effect of carbon on YBCO was demonstrated and it was reported that increasing amount of carbon in the samples resulted in highly microporous structures. Shogo *et. al.* fabricated CO_2 sensors using $CeO/BaCO_3/CuO$ ceramics which have high resistance to humidity and can be used in indoor quality monitoring systems [102-104].

Aims and Motivations

The detailed literature survey led the attention to synthesis of Ba doped CuO and $BaCuO_2$nanomaterials due to their wide applications. Until now $BaCuO_2$ have been synthesized in bulk with wide range of applications in superconducting materials. Litrature is also available on alkali metals doping in TMOs. There is a limited literature available for the synthesis of this $BaCuO_2$, Ba-doped CuO in nanophase via wet chemical approach. There was a thirst to develop a feasible and economic wet chemical process for the synthesis of Ba-doped materials and $BaCuO_2$with the control of size, morphology and composition.

The main goals of the research work are given below,

1. To develop a feasible and economic wet chemical synthesis methodology for single phase nanomaterial.
2. To characterize the product.
3. To investigate the optical, dielectric and thermal properties of synthesized materials.

Chapter 3: Experimental

This section includes the synthesis and characterization of Ba doped CuO and BaCuO$_2$nanomaterilas, followed by physical properties measurements.The chemicals used in the experiments were: BaCO$_3$, and CuO both were of analytical grade purchased from Deajung, Korea andCu(NO$_3$)$_2$.3H$_2$O and Ba(NO$_3$)$_2$were purchased from Merck.Whereas Citric Acid,HNO$_3$ and Ethylene glycol of high purity were purchased from Sigma Aldrich.

3.1. Hydrothermal Synthesis of Ba doped CuO Nanoparticles

A modifiedversion of [105] reported protocol was followed for the fabrication of Ba doped CuO. For the synthesis of Ba doped CuO nanoparticles (with a.1:2 and b. 1:1 for Ba:Cu ratios), Cu(NO$_3$)$_2$.3H$_2$O and Ba(NO$_3$)$_2$were added directly into the two separate autoclaves which were already having required DI water in order to get the desired solutions. After immediate addition of 5M NaOH aq. Solution, autoclaves were kept at 180°C for 6h. After 6h the autoclaves were placed at room temperature for several hours, in order to cool down naturally. Black precipitates of obtained nanomaterials were then subjected to centrifugation for the washing purpose,for numerousintervals with distilled water and then placed in vacuum oven for at 80°C for 24h. The product was pulverizedafterward and further calcined at 500°C for 3h.
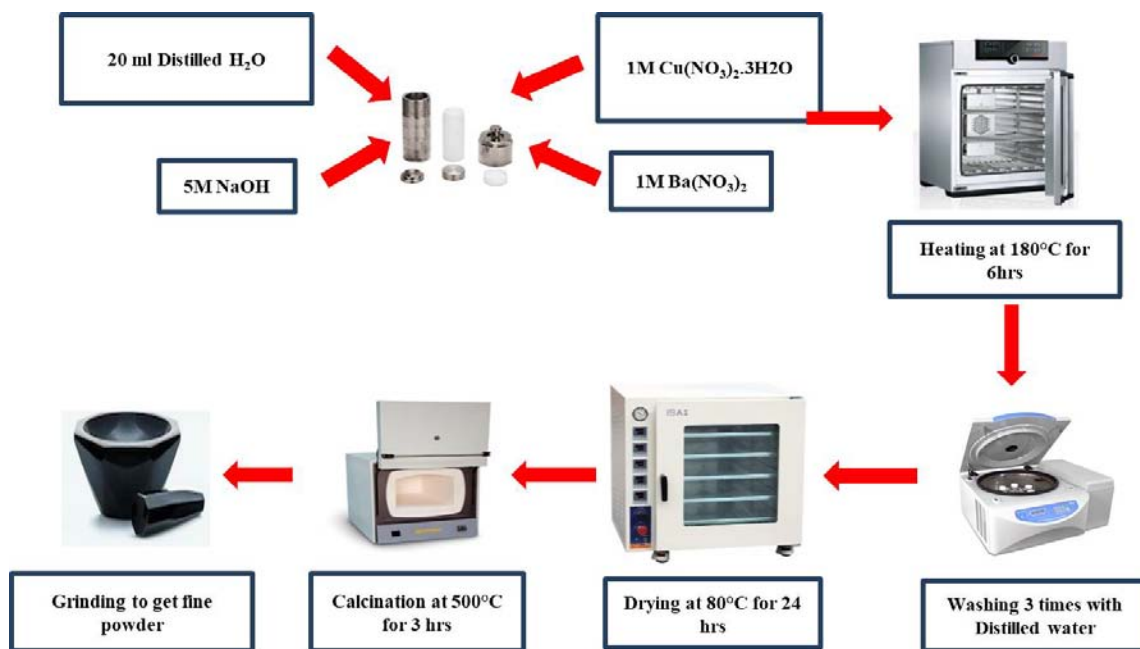
Figure 3.1. Flow sheet diagram for the hydrothermal synthesis of Ba doped CuO

Synthesis of BaCuO$_2$ by Citrate Pyrolysis Method.

Another modified[106]protocol was followed for the fabrication of BaCuO$_2$nanomaterial. In typical procedure, solid BaCO$_3$ and CuO were mixed thoroughly for 5-10 minin agate pastel and mortarand then the resulting precursors were dissolved in HNO$_3$ at about 80ºC to get 0.01M solution. After that 0.3 Maqueous solution of citric acid and 0.1 Maqueous solution of ethylene glycol wereadded to HNO$_3$ solution withconstant stirring. The resulting mixture was heated at90ºC with continuous stirring. Afterwards itwas dried at 150ºC for 24h followed by pulverization and calcinations at various temperatures in order to optimize synthesis condition for BaCuO$_2$ nanoparticles.
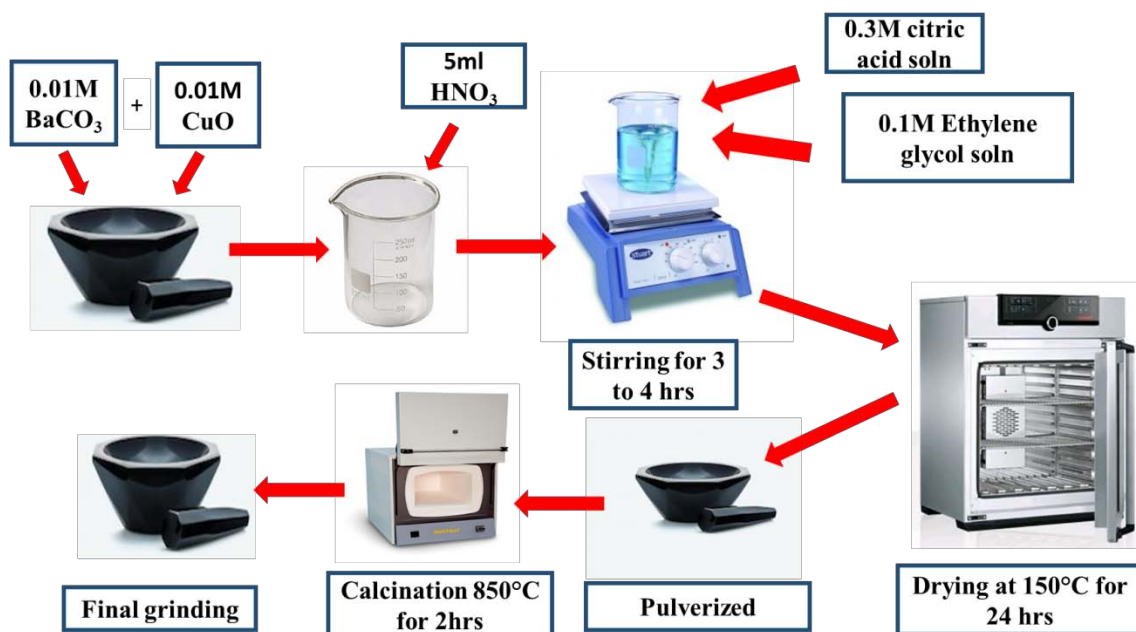
Figure 3.2. Flow sheet diagram for the synthesis of BaCuO$_2$ NPs by Citrate pyrolysis method

3.1. Characterization

XRD patterns for the synthesizedCuO, Ba-doped CuO and for BaCuO$_2$ were recorded using a X-ray diffractometer D8 Discover with CuKα with $\lambda=1.5405$Åin the scan range of $20°<2\theta>80°$.Rietveld refinements were performed for the lattice parameters refimenetsvia Fullprof[107] FESEM and EDSwere performed at Model VEGA 3 TESCAN for morphological studies of the prepared samples and to analyze the elemental composition of the undoped, Ba-doped CuO and BaCuO$_2$ nanoparticles.Samples were prepared by sonicating 1mg of prepared material in 5ml of distilled water. Then put a drop of this solution on glass slide and oven dried at 80°C for 15min. Later on standard coating procedures were performed over these samples.UV-Vis (single beam) spectrophotometer model T60 PG instruments UK, was also employed to check the transmittance for band gap calculations. Samples were prepared by sonicating 1mg of material in 5ml of distilled water. For dielectric properties, pellets of 10mm diameter and 2-3mm thickness were kept between electrodes of Wayne Kerr model 6500 B LCR meter with frequency range 100 Hz to 5MHz.Thermogravimetric

analysis (TGA) was done using DTG-60H System. The samples werethermally treated from 25 °C to 1000 °C at the rate of 10 °C/min under nitrogen,at a flow rate of 50ml/min, in alumina crucibles.

Chapter 4:Result and Discussion

This chapter deals with the result details and discussion over these findings.

Characterization
1. XRPD

XRPD data of pure nanoceramics was recorded and crystal structures were confirmed by comparing with literature, all peaks for pure and doped CuOnanomaterials are indexed with JCPDS card no. 01-089-5897 and $BaCuO_2$ is perfectly matched with the JCPDS card # 01-088-1851. The average crystallite sizes are calculated as 30to 53nm for pure CuO, $Ba_{0.2}Cu_{0.8}O$, $Ba_{0.4}Cu_{0.6}O$ and 70nm for $BaCuO_2$,calculatedby using Scherrer formula.Table 4.1 depicts the lattice parameters, density and cell volume obtained with generalized harmonic description during Rietveld refinement.

Table 4.1 phase density, unit cell volume and crystallite sizes of pure and doped CuOcrytalised in space group **C2/c, #15**

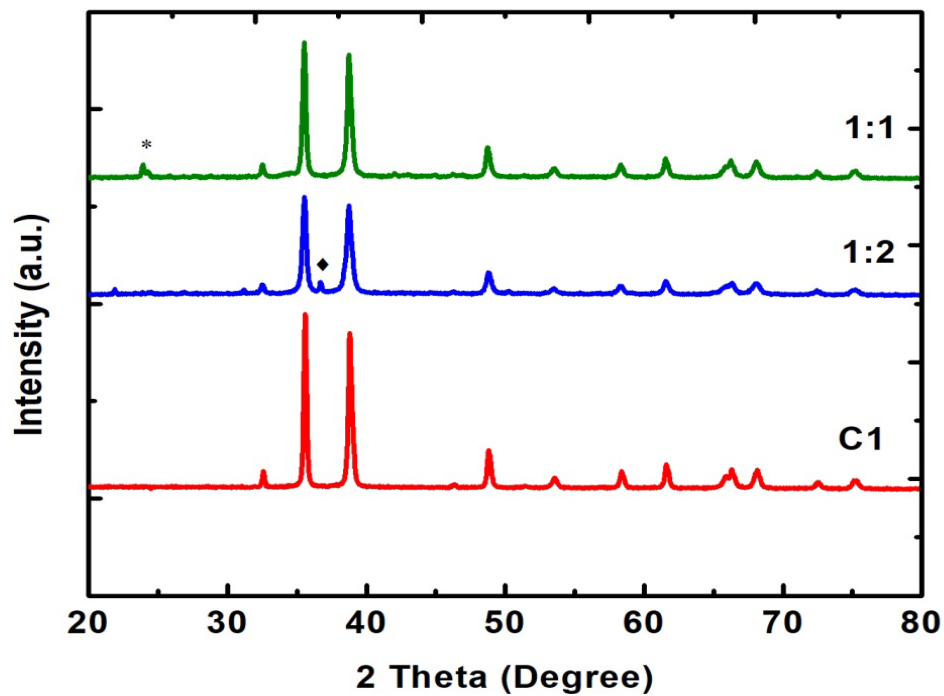| Sample	Lattice parameters (Å)			β (º)	Density (g/cm^3)	Cell Volume (Å^3)	Crystallite size (nm)
	a	**b**	**c**				
Pure CuO	4.6830(3)	3.4231(3)	5.128(4)	99.501(3)	6.517	81.07(1)	53
$Ba_{0.2}Cu_{0.8}O$	4.6824(6)	3.4266(6)	5.1279(7)	99.431(5)	8.975	81.16(2)	42
$Ba_{0.4}Cu_{0.6}O$	4.6807(5)	3.4199(4)	5.1266(5)	99.501(4)	8.927	80.94(2)	30

Figure 4.1 Comparison of XRD pattern of C1(CuO), BC1(1:2), BC2(1:1)
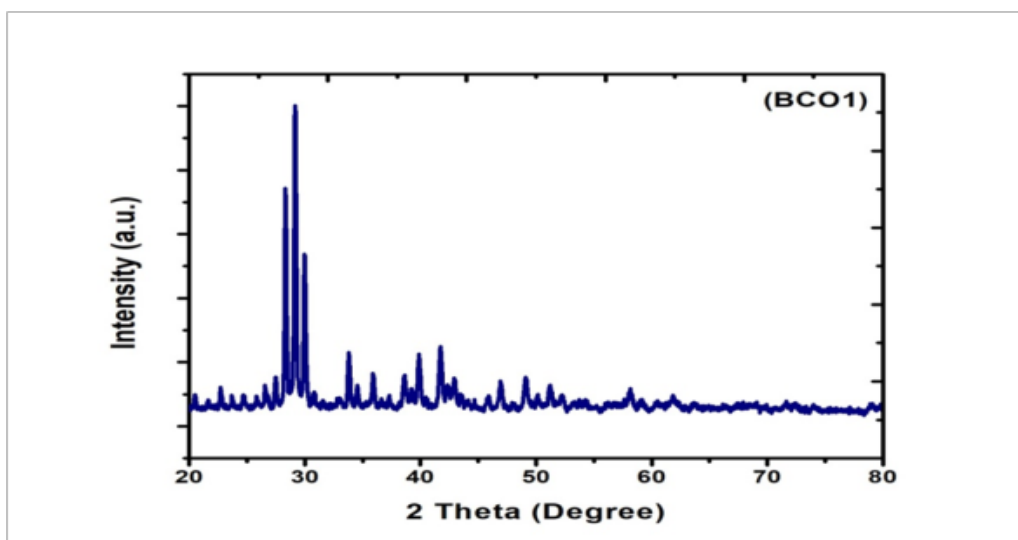
Figure 4.2 XRD Pattern of BCO1 (BaCuO$_2$)
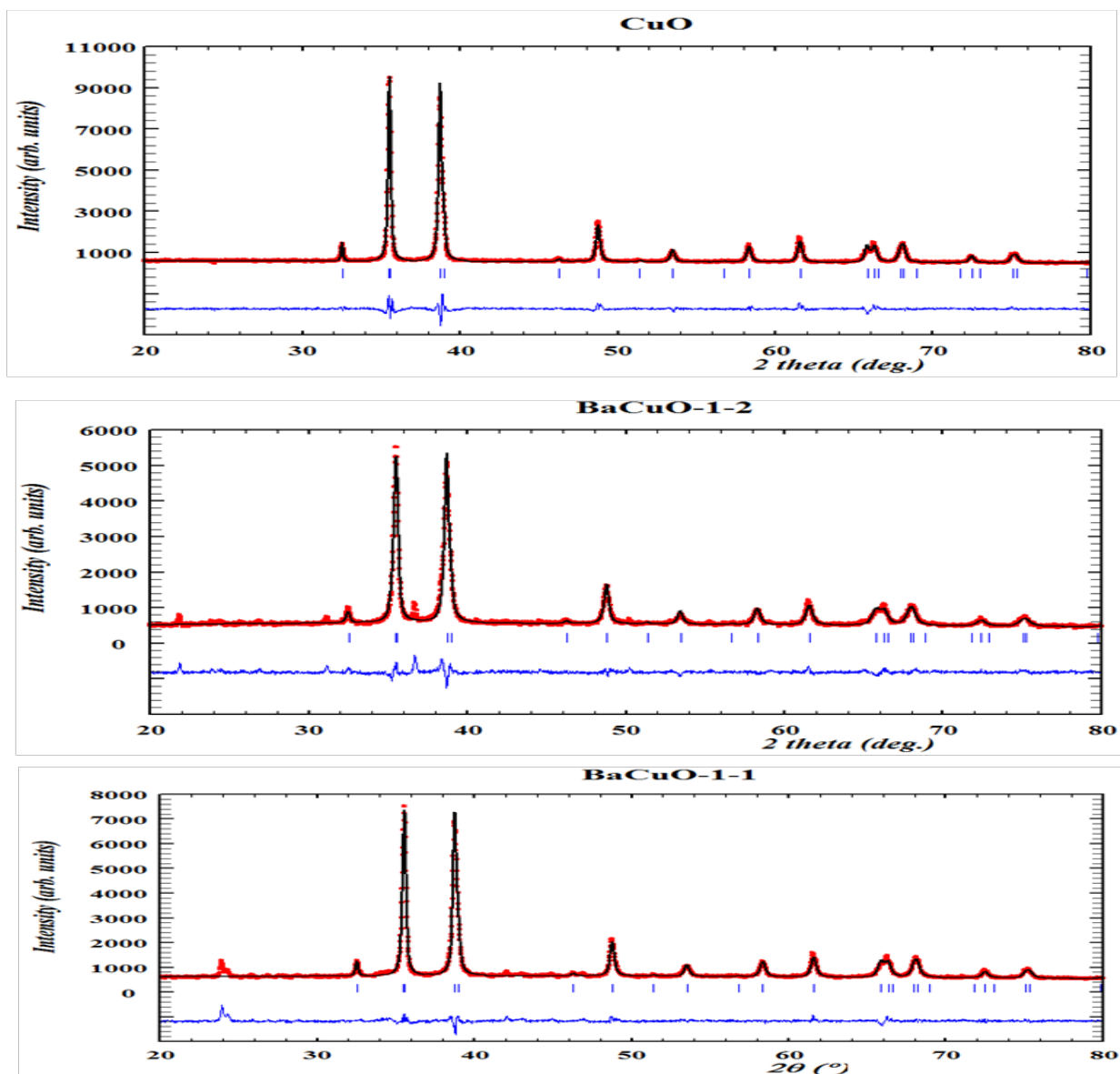
Figures 4.3 Figure showing Rietveld refinements for the pure and Ba doped
nanomaterials.

4.2. SEM

For morphological analysis, the prepared samples were subjected to SEM analysis.
Figure 4.4a shows SEM image of pure CuO nanoparticles having spherical morphology
in which the particles are agglomerated due to hygroscopic behavior of the sample. The
average particle size was found to be ~70 nm. Fig 4.4b shows that $Ba_{0.2}Cu_{0.8}O$ exhibit
cubical morphology which has average particles size of about ~54 nm. Fig 4.4c shows
SEM image of $Ba_{0.4}Cu_{0.6}O$ which shows rod like morphology with average ~67nm

daimeter. While the Fig 4.4d is for $BaCuO_2$ nanoparticles with average particle size of ~33nm.This type of doped TMO was observed in Ba-doped-ZnO. In 2016 Kekeli N Konounoticed that the crystal became compact by increasing the dopant level. However, the crystallite sizes of the nanoparticles decrease[39].In the same year they reported that the morphology of TMOs (transition metal oxide)became modified with Ba-doping. They observed that the undopedZnO morphology has been changed upon modification with Ba. This morphological change can be attributed to the presence of the Ba element, which modifies the raspberry-like structure of undopedZnO to the flower-like structure of $ZnOBa_2$[37].
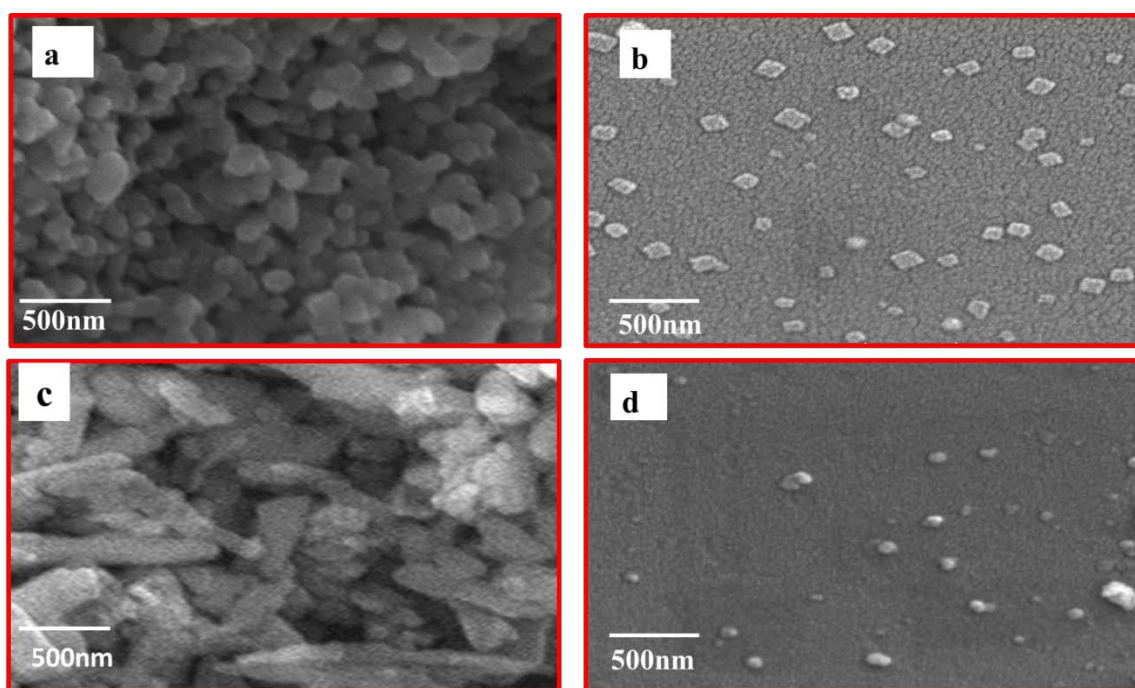
Figure 4.4. SEM images of a) CuO b)$Ba_{0.2}Cu_{0.8}O$ c) $Ba_{0.4}Cu_{0.6}O$ d) $BaCuO_2$

4.3. Energy Dispersive X-Ray Spectroscopy (EDX)

The elemental analysis was carried out by EDX equipped with FESEM. Figure 4.5a-d show EDX spectra of pure CuO, Ba doped CuO and $BaCuO_2$nanomaterialsrepresenting that the samples contain only O,Cu and Ba. EDX data of CuO, $Ba_{0.2}Cu_{0.8}O$, $Ba_{0.4}Cu_{0.6}O$, $BaCuO_2$is given in the figure 4.5 and table 4.1.
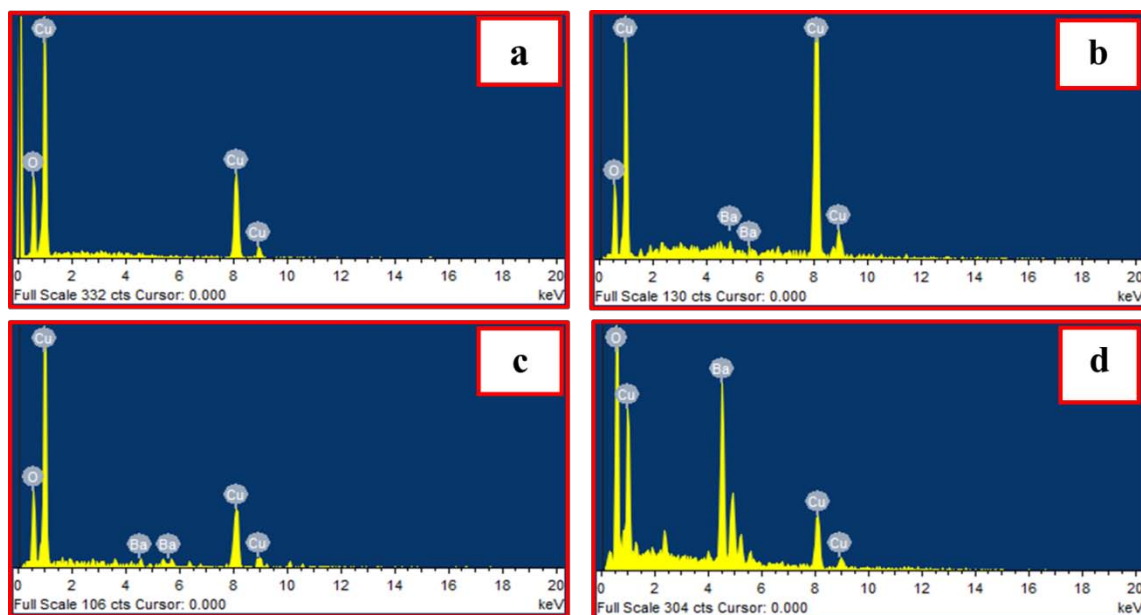
Figure 4.5 EDX pattern ofa) pure CuO b) $Ba_{0.2}Cu_{0.8}O$ c) $Ba_{0.4}Cu_{0.6}O$ d) $BaCuO_2$

Table 4.2.EDX data of a) pure CuO b) $Ba_{0.2}Cu_{0.8}O$ c) $Ba_{0.4}Cu_{0.6}O$ d) $BaCuO_2$

Sample	Element	Average wt %
CuO	O	30.06
	Cu	69.94
$Ba_{0.2}Cu_{0.8}O$	O	23.5
	Cu	74.64
	Ba	1.86
$Ba_{0.4}Cu_{0.6}O$	O	33.44
	Cu	62.43
	Ba	4.13
$BaCuO_2$	O	23.28
	Cu	22.65
	Ba	54.2

Physical Properties

Optical properties were investigated for band gap calculation and dielectric properties for dielectric loss, dielectric constant, AC conductivity and tan losscalculations. Further TGA was also performed to find out the average weight loss of synthesized materials as a function of temperature.

1. Optical Properties

UV-Vis spectroscopy is used to investigate the absorbance spectra of synthesized materials was recorded.**Principle**:When a sample is exposed to light energy, that matches the energy difference between possible electronic transitions. A fraction of light energy would be absorbed by the molecules. A spectrometer records the degree of absorption by the sample at different wavelength, and the resulting plot between absorbance and wavelength is known as absorption spectrum.
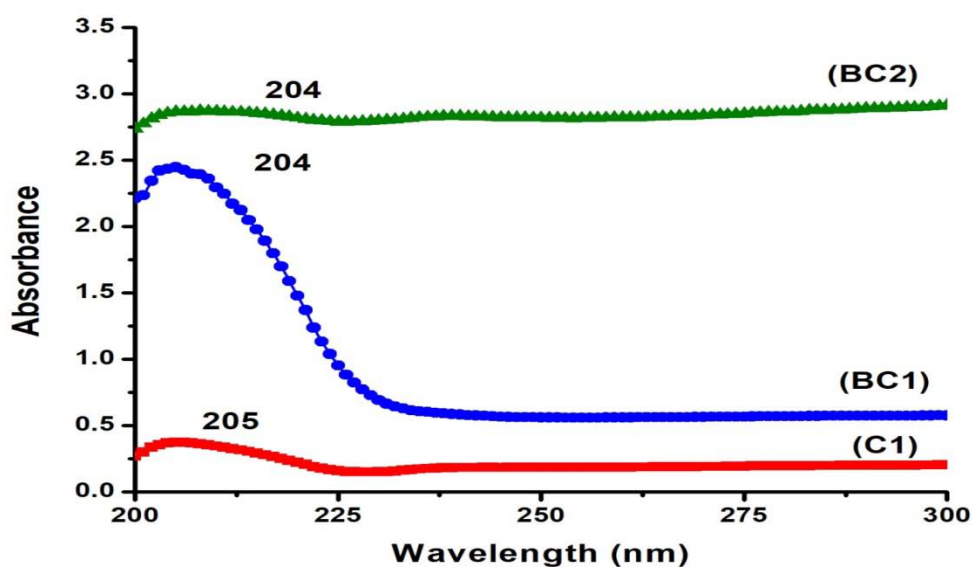
Figure 4.6 Absorbance spectra of a) C1 b) BC1 c) BC2

Band Gap

A band gap is the distance between valance band and the conduction band of an electron. The optical band gap of the material can be determined by a tauc plot. UV-Vis spectroscopy revealed band gab between 5.74 eV for undopedCuO, the band gap for $Ba_{0.2}Cu_{0.8}O$ was greater than 6 eV, and for $Ba_{0.4}Cu_{0.6}O$ was 5.8.eV while the band gap for $BaCuO_2$ was 5.77eV. These results indicated that least concentration of dopant gave the highest band gap.
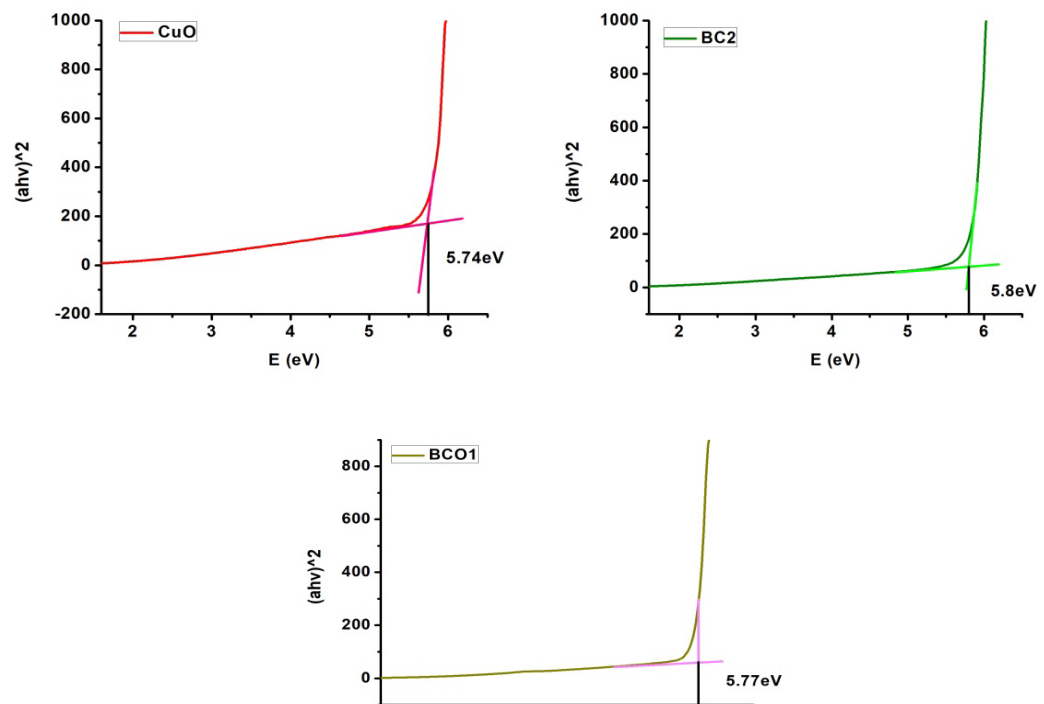
Figure 4.7 Band gap calculation of CuO, $Ba_{0.4}Cu_{0.6}O$, and $BaCuO_2$

Dielectric Properties

To study the application of prepared materials as capacitors, dielectric properties were carried out using LCR meter and processing the obtained data by using different equations discussed in upcoming sections. Different parameters investigated are AC conductivity, dielectric loss, dielectric constant, and tangent loss.

Dielectric parameter could be represented as[108].

$$\varepsilon^* = \varepsilon' - i\varepsilon''$$

ε' is the real part which is dielectric constant and $i\varepsilon''$ is an imaginary part which is dielectric loss. This part explain the ability to transfer the charges or ability to store the charges of material. The real part could be calculated as,

$$\varepsilon' = \frac{C \cdot d}{A \cdot \varepsilon_o}$$
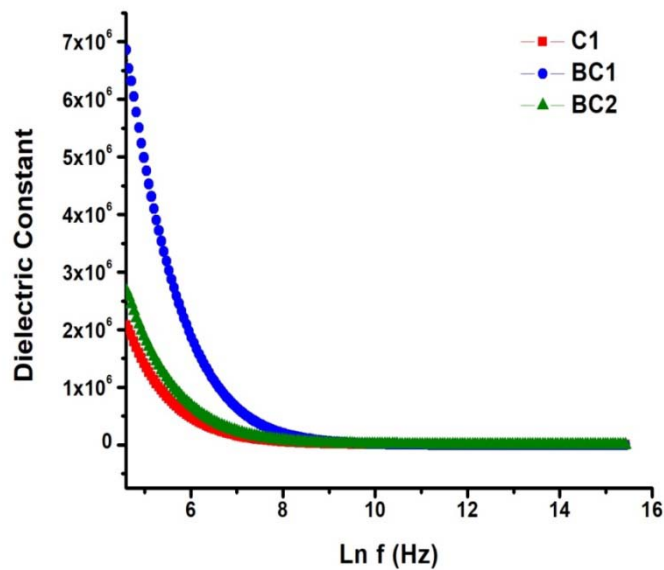
Figure 4.8 Dielectric constant of a) CuO b) $Ba_{0.2}Cu_{0.8}O$ c) $Ba_{0.4}Cu_{0.6}O$ d) $BaCuO_2$

Where, C is capacitance, d refers to thicknes (nm), A referst to surface area (m^2), ε_o is the permitivity of free space (8.85×10^{-12}). It was perceived that as the frequency increases dielectric constant of the material decreases BC1 shows higher dielectric constants values that are 7×10^6. It was seen that dielectric constant shows the frequency dependent behaviour as frequency increases dielectric constant decreases. Dielectric constant is actually dependent on grain boundries that are created with in the material when external electrical charge is applied and high polarization achieved at low frequency as the frequency increases the priviously formed dipole fail to arrange

themselves with fluctuating current so dielectric constant decreases and after certain value it become constant. It was seen by Fig 4.8. That as we increase the amount of metal oxides in material dielectric constant decreases it is due to poor separating boundries formation and also due to the porosity and defects. Dielectric loss is imaginary part that shows the heat dessipation and methematically can be calculated as,

$$\varepsilon'' = \varepsilon' \times Dissipation\ factor$$
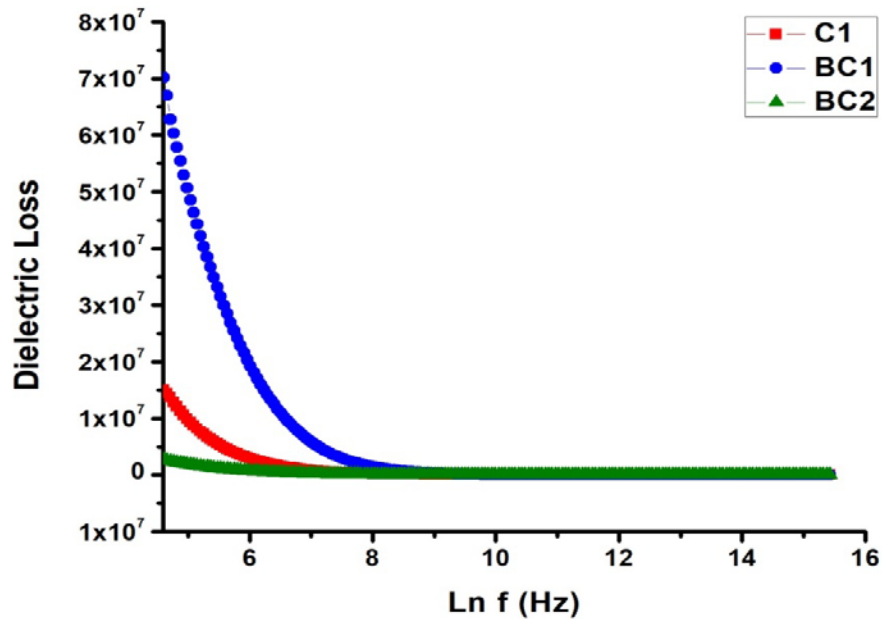
Figure 4.9 Dielectric Loss of a) CuO, b) $Ba_{0.2}Cu_{0.8}O$, c) $Ba_{0.4}Cu_{0.6}O$

Fig 4.9. shows the dielectric loss of values of pure and Ba doped CuO nanomaterials. An unexpected behaviour was observed in case of dielectric loss. Where BC2 shows the lowest dielectric constant which is contradictory to dielectric constant trend. As frequency increases atom did not show rapid electron transfer due to which dielectric loss value also decreases. As the frequency increases less energy consumed for hopping of electrons and heat loss also become less at higher frequency [109]. BC1 shows highest dielectric loss values 7×10^7.

Figure 4.10 shows the dielectric loss measurements of all synthesized materials that is actually the heat loss expressed in terms of tan loss, mathematically it can be expressed by following formula

$$tan\delta = \frac{\varepsilon''}{\varepsilon'}$$

Tan loss (tan δ) is relative measure of energy loss. Resonance peaks of BC1 was observed with increasing amplitude at low frequency it is actually the point at which frequency of hopping electrons resonanate with external electric field as shown in Fig 4.10 [110].Values observed in case of tan loss were low and same periodic trend was observed as for dielectric constant.
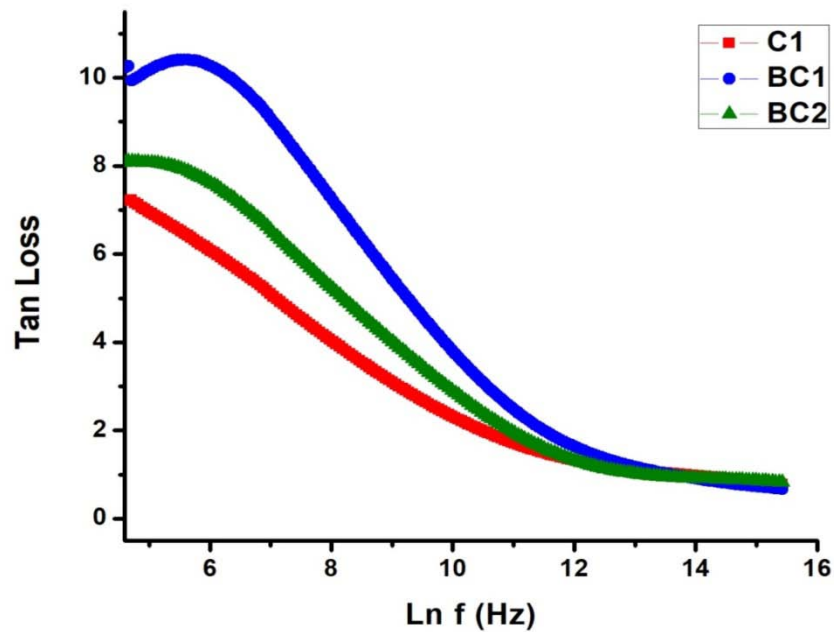
Figure 4.10 Tan Loss of a) CuO, b) $Ba_{0.2}Cu_{0.8}O$, c) $Ba_{0.4}Cu_{0.6}O$

AC conductivity of the material is its ability to allow the passage of current. When the external field is applied on the material they allign themselves and their hopping frequency resonate with the external frequency it could be measured as [111]

$$\sigma_{ac} = 2\pi f\varepsilon'\varepsilon_o tan\delta$$
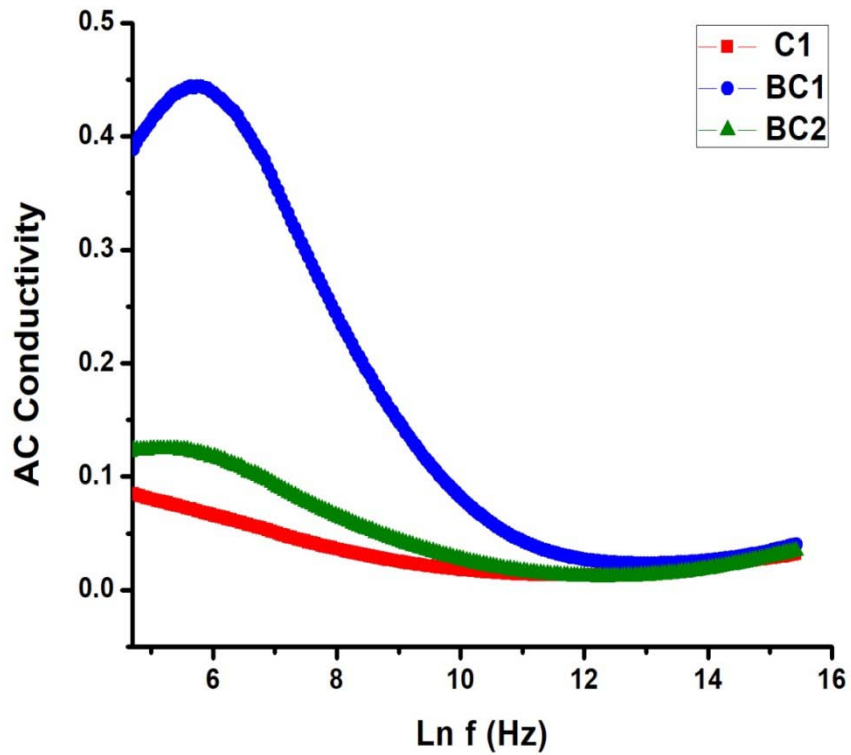
Figure 4.11 AC Conductivity of a) CuO, b) $Ba_{0.2}Cu_{0.8}O$ c) $Ba_{0.4}Cu_{0.6}O$

Fig 4.11. shows that BC1 shows higher AC conductivity at low frequency as charge carrier easily allign themselves according to external applied field and it decreases as frequency increases as charge carrier did not get enough time to arrange themselves they move rendomly due to which AC conductivity decreases.
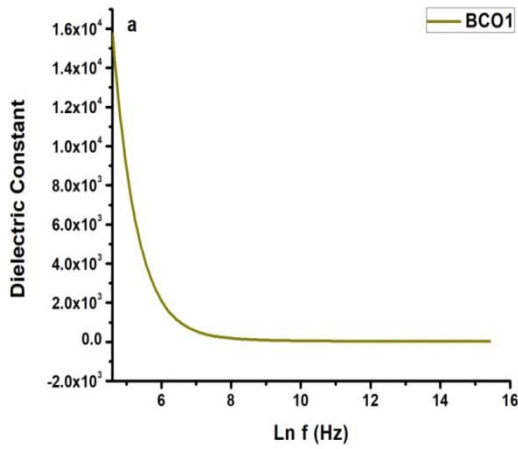
Dielectric constant of $BaCuO_2$
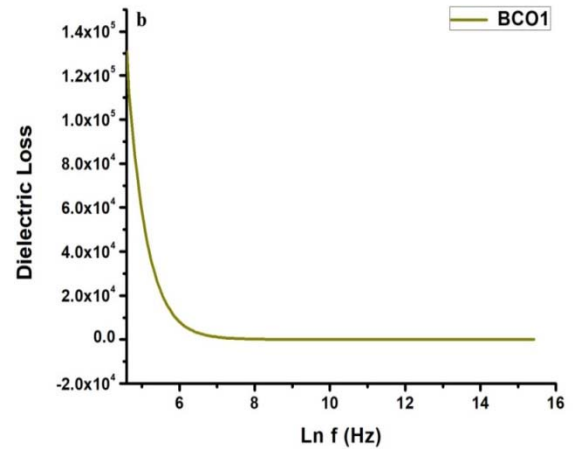
Dielectric loss of $BaCuO_2$
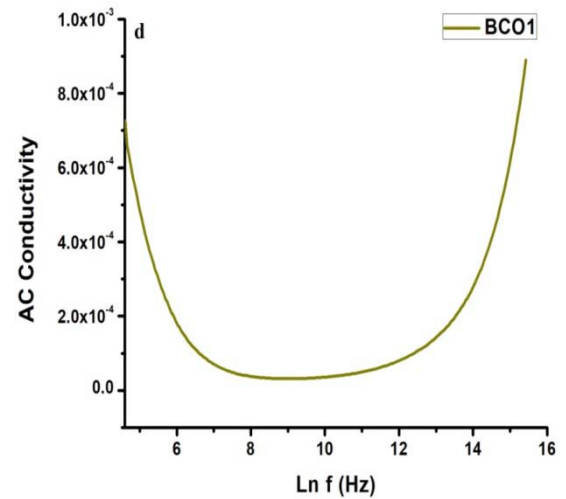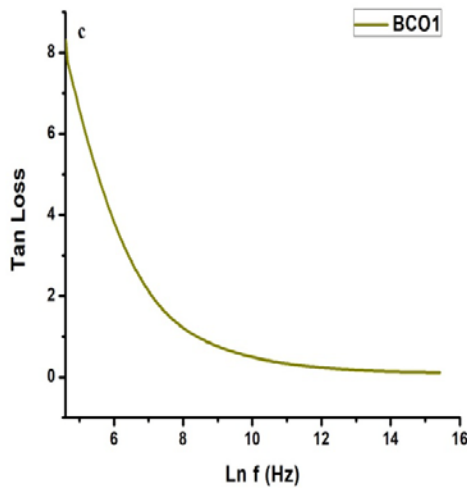
In dielectric properties of $BaCuO_2$ we can observe the similar trend for dielectric constant, dielectric loss and tan loss as that for Ba-doped CuO with much lower

Figure 4.12 DC, DL, TL, and ac Conductivity of $BaCuO_2$

values.The value of dielectric constant is 1.6 x 10^4 value of dielectric loss is 1.4 x 10^5 and the value of tan loss is 8.While ac conductivity shows an unusual trend which first decreases from 7 x 10^{-4} upto 1 x 10^{-4} with increase in frequency then become constant for short interval and it again tend to increases at higher frequency from 1 x 10^{-4} upto 9 x 10^{-3}.

Thermogravimetric Analysis (TGA)

Thermal analysis was carried out to find the decomposition temperature of synthesized materials. It was carried to investigate the decomposition temperature of undoped and Ba-doped-CuO and $BaCuO_2$. TG curve represented by red line is for pure CuO. No upward or downward peaks can be observed in DTA curve which means that no exo or endothermic reaction taking place and hence no phase transformation is happening. Which means the sample is not degraded. The mass of sample is gradually decreasing with temperature. The results exhibited that there was no prominentmass lossin the TG curves, evidencing the presence of CuO, which does not disintegrate within this temperature range.The total mass loss is 4%.which might be due to removal of moisture.
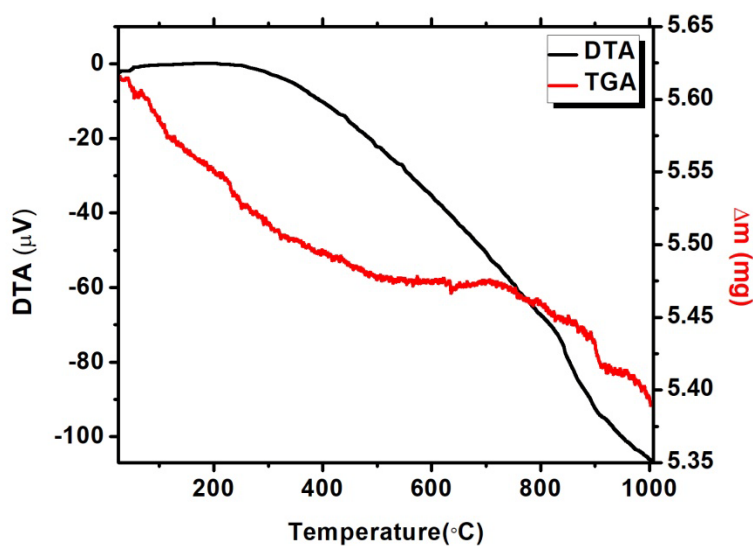
Figure 4.13 TG/DTA curve of CuO

TG curve with for $Ba_{0.2}Cu_{0.8}O$ is represented by blue. The mass loss in this is 9%. Which means the stability of CuO decreases with Ba doping.
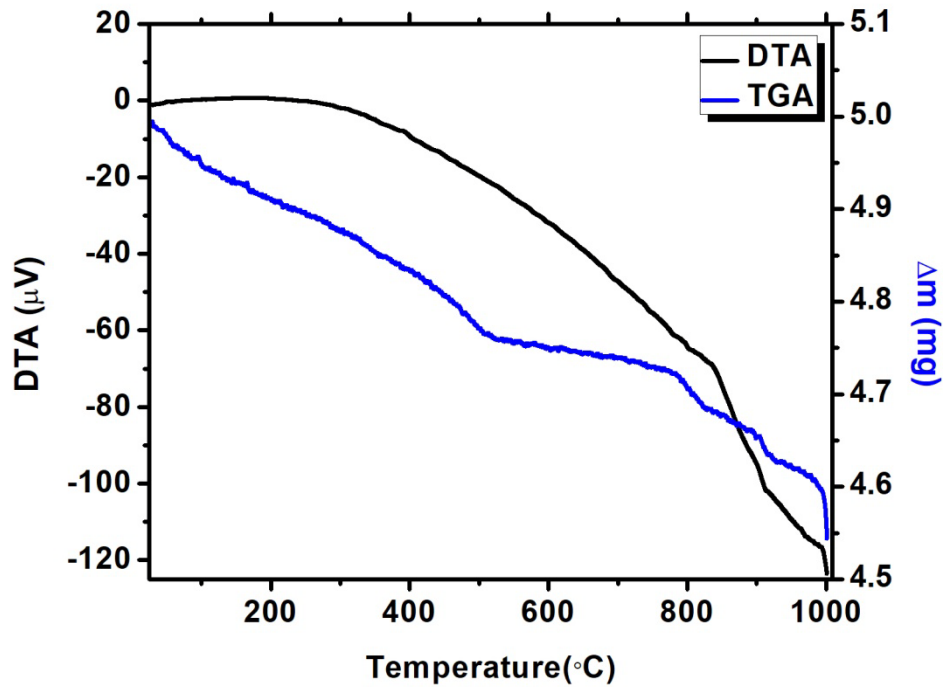
Figure 4.14 TG/DTA curve of $Ba_{0.2}Cu_{0.8}O$

TGA curve of $Ba_{0.4}Cu_{0.6}O$ is represented by green. DTA curve show the same trend as for $Ba_{0.2}Cu_{0.8}O$. the total mass loss in this case is 5%.
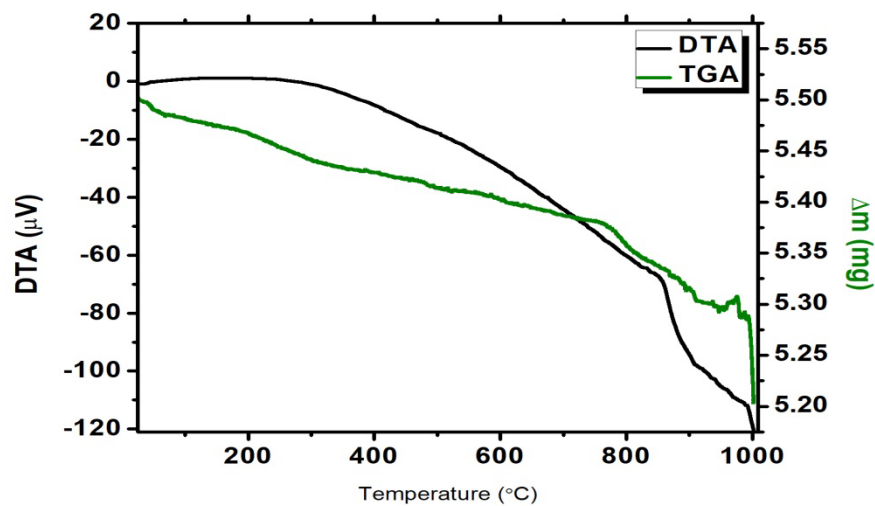
TG   curve

Figure 4.15 TG/DTA curve of $Ba_{0.4}Cu_{0.6}O$
of $BaCuO_2$ shows totally different behavior. We can observe a sharp mass loss at 275°C.

From DTA curve we can observe an exotherm at the same temperature which means weight loss. After that there is an increase in mass which might be due to absorption of oxygen from the environment. Then at 800°C TG curve shows sharp decrease in mass. 12% mass loss can be observed in this case. There is a substantial scatter of the data in the literature on the melting temperatures and mechanisms for $BaCuO_2$. $BaCuO_2$ melts congruently at 1020°C [112], via a complex mechanism at 1000–1010°C [113], congruently with oxygen loss at 1005°C [114], and incongruently with decomposition to BaO at 975°C [115] and to Ba2CuO3 at 988°C [116], and with the formation of two liquids at 1016°C [117]. So according to this literature mass loss can be due to one of the following conversions

$$1\text{-}BaCuO_2 \quad BaO + CuO$$

$$2\text{-}\ 2BaCuO_2 \quad Ba_2CuO_3 + CuO$$
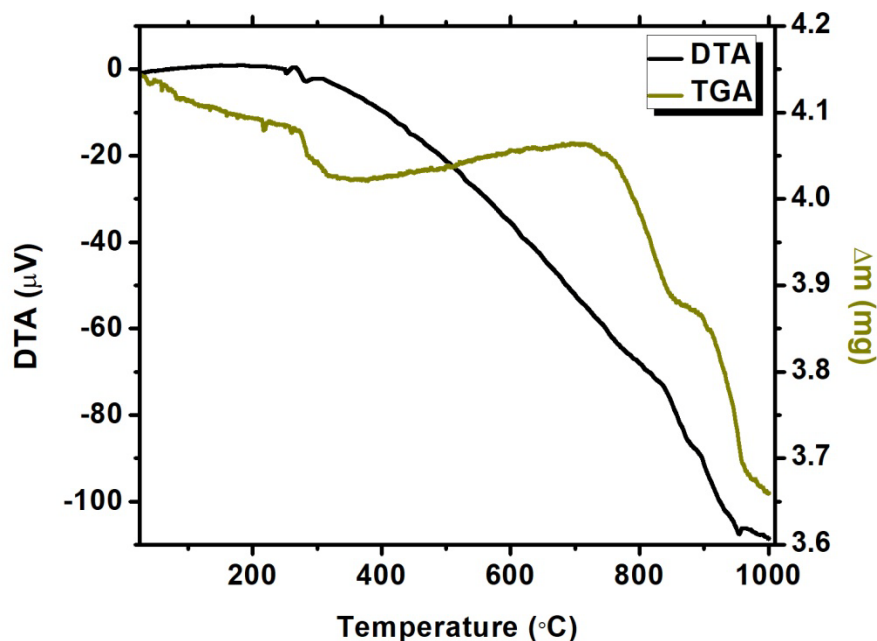
Figure 4.16 TG/DTA curve of $BaCuO_2$

Following graph shows the % mass loss of undoped, Ba doped CuOand $BaCuO_2$ respectively
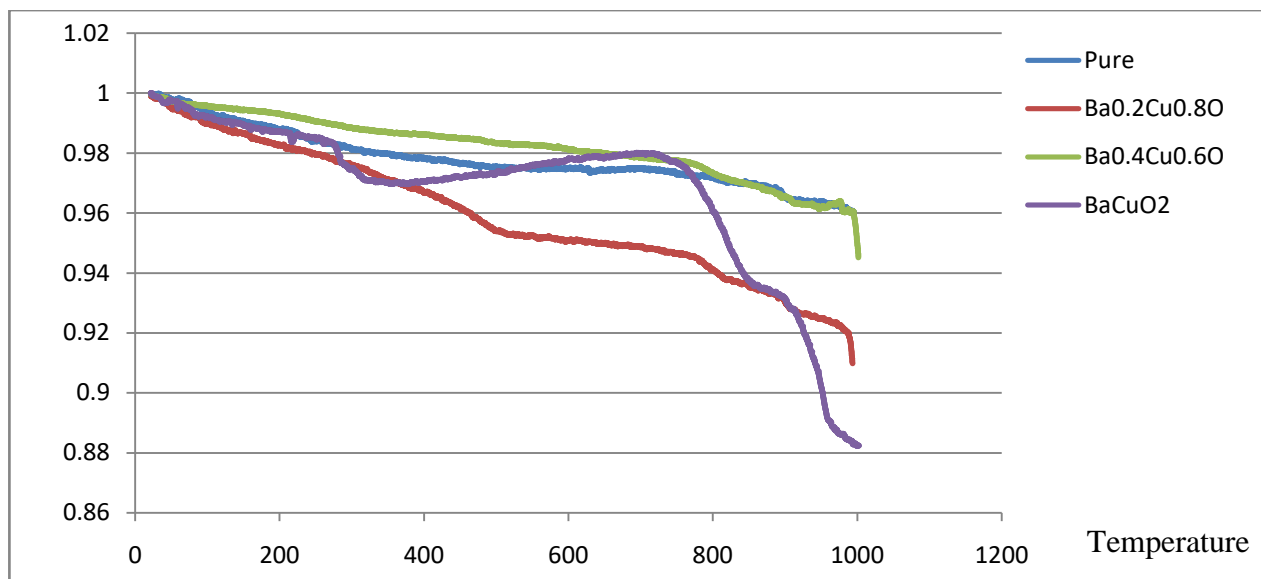
Figure 4.17 % mass loss of a) CuO b) $Ba_{0.2}Cu_{0.8}O$ c) $Ba_{0.4}Cu_{0.6}O$ d) $BaCuO_2$

Conclusion

UmdopedCuO and Ba-doped-CuO ($0.2 \leq$ x ≤ 0.4)nanomaterials has been synthesized via simple, feasible and economical hydrothermal method and BaCuO $_2$nanoparticles has been synthesized by citrate pyrolysis method. Successful synthesis was confirmed with the help of XRD, SEM and EDX techniques.A peak shift was observed for Ba-doped materials in XRD pattern. XRD also confirm the successful synthesis of single phase $BaCuO_2$ nanoparticles. Average crystallite size calculated by Sherrer formula decreases with Ba-doping from 53.5nm to 30nm. And crystallite size for $BaCuO_2$ was 70nm.SEM was performed for morphological analysis and EDX for elemental analysis. The results of SEM depicted that morphology changes from spherical to cubical to nanotubes from Undoped to $Ba_{0.2}Cu_{0.8}O$ to $Ba_{0.4}Cu_{0.6}O$ respectively. This change in morphology is also attributed to Ba-doping.EDX results confirm the doping of Ba in CuO nanoparticles with 2 to 4 average weight percent respectively. Optical dielectric and thermal properties of the synthesized materials were studied. UV-vis was used to study band gap of synthesized material which shows that the band gap increases with Ba-doping in CuO nanoparticles. 2% Ba-doping show highest band gap, greater than 6 eV. While band gap of BaCuO $_2$ nanoparticles is 5.7 which was approximately equal to that of CuOnanoparticles. Dielectric constant of 2% doped material was highest of 7 x 10^6 all

which means that it has more ability to store more charge than 4% Ba-doping thus have higher capacitive nature. While $BaCuO_2$ showed lowest band gap1.6 x $10^{4.}$ While the dielectric loss or synthesized material show unexpected results then dielectric constant. Which shows that 4% Ba-doped material showed lowest dielectric loss. Which means that it loss less energy during AC fluctuation. TGA results showed that our synthesized materials are thermally stable upto 1000°C as very less % mass loss was observed 4% to 12% only. So the results showed that 2 % Ba doping show best dielectric properties and can be used as capacitors.

References

[1]   N. Taniguchi, "On the basic concept of nano-technology," in *Proc. Intl. Conf. Prod. London, 1974*, 1974.

[2]   K. E. Drexler, *Nanosystems: molecular machinery, manufacturing, and computation*: John Wiley & Sons, Inc., 1992.

[3]   E. Llobet, "Gas sensors using carbon nanomaterials: A review," *Sensors and Actuators B: Chemical,* vol. 179, pp. 32-45, 2013.

[4]   A. Alagarasi, "Chapter-Introduction To Nanomaterials," 2011.

[5]   K. Scida, P. W. Stege, G. Haby, G. A. Messina, and C. D. García, "Recent applications of carbon-based nanomaterials in analytical chemistry: critical review," *Analytica chimica acta,* vol. 691, pp. 6-17, 2011.

[6]   Q. Zhang, J. Q. Huang, W. Z. Qian, Y. Y. Zhang, and F. Wei, "The road for nanomaterials industry: A review of carbon nanotube production, post-treatment, and bulk applications for composites and energy storage," *Small,* vol. 9, pp. 1237-1265, 2013.

[7]   E. Roduner, "Size matters: why nanomaterials are different," *Chemical Society Reviews,* vol. 35, pp. 583-592, 2006.

[8]   Q. A. Pankhurst, J. Connolly, S. Jones, and J. Dobson, "Applications of magnetic nanoparticles in biomedicine," *Journal of physics D: Applied physics,* vol. 36, p. R167, 2003.

[9]   Q. H. Wang, K. Kalantar-Zadeh, A. Kis, J. N. Coleman, and M. S. Strano, "Electronics and optoelectronics of two-dimensional transition metal dichalcogenides," *Nature nanotechnology,* vol. 7, p. 699, 2012.

[10]   D. Huang, F. Liao, S. Molesa, D. Redinger, and V. Subramanian, "Plastic-compatible low resistance printable gold nanoparticle conductors for flexible electronics," *Journal of the electrochemical society,* vol. 150, pp. G412-G417, 2003.

[11]   V. Biju and M. A. Khadar, "Analysis of AC electrical properties of nanocrystalline nickel oxide," *Materials Science and Engineering: A,* vol. 304, pp. 814-817, 2001.

[12]   V. Biju and M. A. Khadar, "DC conductivity of consolidated nanoparticles of NiO," *Materials research bulletin,* vol. 36, pp. 21-33, 2001.

[13]   T. M. Tritt and M. Subramanian, "Thermoelectric materials, phenomena, and applications: a bird's eye view," *MRS bulletin,* vol. 31, pp. 188-198, 2006.

[14]   G. Singh, *Processing, Properties, and Design of Advanced Ceramics and Composites* vol. 259: John Wiley & Sons, 2016.

[15]   X. Huang and P. Jiang, "Core–shell structured high-k polymer nanocomposites for energy storage and dielectric applications," *Advanced Materials,* vol. 27, pp. 546-554, 2015.

[16]   P. Barber, S. Balasubramanian, Y. Anguchamy, S. Gong, A. Wibowo, H. Gao*, et al.*, "Polymer composite and nanocomposite dielectric materials for pulse power energy storage," *Materials,* vol. 2, pp. 1697-1733, 2009.

[17]   R. Pal, *Electromagnetic, mechanical, and transport properties of composite materials*: CRC Press, 2014.

[18]   C. Suryanarayana and M. Grant Norton, "„X-Ray Diffraction: a practical approach "Springer," *New York,* 1998.

[19]   R. Das, E. Ali, and S. B. Abd Hamid, "CURRENT APPLICATIONS OF X-RAY POWDER DIFFRACTION-A REVIEW," *Reviews on Advanced Materials Science,* vol. 38, 2014.

[20]   S. Charurvedi and P. N. Dave, "Microscopy in Nanotechnology," 2012.

[21]   A. J. Nozik, G. Conibeer, and M. C. Beard, *Advanced concepts in photovoltaics*: Royal Society of Chemistry, 2014.

[22]   P. D. Ngo, "Energy dispersive spectroscopy," in *Failure Analysis of Integrated Circuits*, ed: Springer, 1999, pp. 205-215.

[23]   J. Torrent and V. Barron, "Diffuse reflectance spectroscopy," *Methods of soil analysis. Part,* vol. 5, pp. 367-387, 2008.

[24]   R. López and R. Gómez, "Band-gap energy estimation from diffuse reflectance measurements on sol–gel and commercial TiO2: a comparative study," *Journal of sol-gel science and technology,* vol. 61, pp. 1-7, 2012.

[25]   U. A. Bakshi and V. U. Bakshi, *Electrical engineering*: Technical Publications, 2009.

[26]   P. G. Wolynes and V. Lubchenko, *Structural glasses and supercooled liquids: Theory, experiment, and applications*: John Wiley & Sons, 2012.

[27]   H. Song, K. Shah, E. Doroodchi, T. Wall, and B. Moghtaderi, "Analysis on chemical reaction kinetics of CuO/SiO2 oxygen carriers for chemical looping air separation," *Energy & Fuels,* vol. 28, pp. 173-182, 2013.

[28]   T. Thongtem, N. Tipcompor, A. Phuruangrat, and S. Thongtem, "Characterization of SrCO3 and BaCO3 nanoparticles synthesized by sonochemical method," *Materials Letters,* vol. 64, pp. 510-512, 2010.

[29]   A. Zelati, A. Amirabadizadeh, and A. Kompany, "Preparation and characterization of barium carbonate nanoparticles," *International Journal of Chemical Engineering and Applications,* vol. 2, p. 299, 2011.

[30]   M.-G. Ma, Y.-J. Zhu, G.-F. Cheng, and Y.-H. Huang, "Fabrication and characterization of BaCO3 nanostructures," *materials letters,* vol. 62, pp. 3110-3113, 2008.

[31]   S. Walia, S. Balendhran, H. Nili, S. Zhuiykov, G. Rosengarten, Q. H. Wang*, et al.*, "Transition metal oxides–Thermoelectric properties," *Progress in Materials Science,* vol. 58, pp. 1443-1489, 2013.

[32]   W. B. Ingler Jr and S. U. Khan, "Photoresponse of spray pyrolytically synthesized magnesium-doped iron (III) oxide (p-Fe2O3) thin films under solar simulated light illumination," *Thin Solid Films,* vol. 461, pp. 301-308, 2004.

[33]   R. Zamiri, B. Singh, I. Bdikin, A. Rebelo, M. S. Belsley, and J. Ferreira, "Influence of Mg doping on dielectric and optical properties of ZnO nano-plates prepared by wet chemical method," *Solid State Communications,* vol. 195, pp. 74-79, 2014.

[34]   J. E. Son, J. Chattopadhyay, and D. Pak, "Electrocatalytic performance of Ba-doped TiO2 hollow spheres in water electrolysis," *international journal of hydrogen energy,* vol. 35, pp. 420-427, 2010.

[35]   K. Vijayalakshmi and D. Sivaraj, "Synergistic antibacterial activity of barium doped TiO 2 nanoclusters synthesized by microwave processing," *RSC Advances,* vol. 6, pp. 9663-9671, 2016.

[36]   G. Srinet, R. Kumar, and V. Sajal, "High Tc ferroelectricity in Ba-doped ZnO nanoparticles," *Materials Letters,* vol. 126, pp. 274-277, 2014.

[37]   K. N'Konou, M. Haris, Y. Lare, M. Baneto, K. Napo, and P. Torchio, "Effect of barium doping on structural and optical properties of zinc oxide nanoparticles synthesized by microwave hydrothermal method," *physica status solidi (b),* vol. 253, pp. 260-266, 2016.

[38]   R. Zamiri, H. M. Chenari, H. Moafi, M. Shabani, S. Salehizadeh, A. Rebelo*, et al.*, "Ba-doped ZnO nanostructure: X-ray line analysis and optical properties in visible and low frequency infrared," *Ceramics International,* vol. 42, pp. 12860-12867, 2016.

[39]   K. N'KONOU, M. Haris, Y. Lare, M. Baneto, and K. Napo, "Effect of barium doping on the physical properties of zinc oxide nanoparticles elaborated via sonochemical synthesis method," *Pramana,* vol. 87, p. 4, 2016.

[40]   B. Shirdel and M. A. Behnajady, "Sol-gel synthesis of Ba-doped ZnO nanoparticles with enhanced photocatalytic activity in degrading Rhodamine B under UV-A irradiation," *Optik-International Journal for Light and Electron Optics,* vol. 147, pp. 143-150, 2017.

[41]   T. Omata, T. Fuke, and S. Otsuka-Yao-Matsuo, "Hydration behavior of Ba2Sc2O5 with an oxygen-deficient perovskite structure," *Solid State Ionics,* vol. 177, pp. 2447-2451, 2006.

[42]   A. Beauger, J. Mutin, and J. Niepce, "Synthesis reaction of metatitanate BaTiO3," *Journal of materials science,* vol. 18, pp. 3041-3046, 1983.

[43]   S. Urek and M. Drofenik, "The hydrothermal synthesis of BaTiO3 fine particles from hydroxide–Alkoxide precursors," *Journal of the European Ceramic Society,* vol. 18, pp. 279-286, 1998.

[44]   D. Chen and X. Jiao, "Solvothermal synthesis and characterization of barium titanate powders," *Journal of the American Ceramic Society,* vol. 83, pp. 2637-2639, 2000.

[45]   S. W. Lu, B. I. Lee, Z. L. Wang, and W. D. Samuels, "Hydrothermal synthesis and structural characterization of BaTiO3 nanocrystals," *Journal of Crystal Growth,* vol. 219, pp. 269-276, 2000.

[46]   L. Simon-Seveyrat, A. Hajjaji, Y. Emziane, B. Guiffard, and D. Guyomar, "Re-investigation of synthesis of BaTiO3 by conventional solid-state reaction and oxalate coprecipitation route for piezoelectric applications," *Ceramics international,* vol. 33, pp. 35-40, 2007.

[47]   T. Karaki, K. Yan, T. Miyamoto, and M. Adachi, "Lead-free piezoelectric ceramics with large dielectric and piezoelectric constants manufactured from BaTiO3 nano-powder," *Japanese Journal of Applied Physics,* vol. 46, p. L97, 2007.

[48]   C.-Y. Chang, C.-Y. Huang, Y.-C. Wu, C.-Y. Su, and C.-L. Huang, "Synthesis of submicron BaTiO3 particles by modified solid-state reaction method," *Journal of Alloys and Compounds,* vol. 495, pp. 108-112, 2010.

[49]   S. Fuentes, R. Zárate, E. Chávez, P. Munoz, M. Ayala, R. Espinoza-González*, et al.*, "Synthesis and characterization of BaTiO3 nanoparticles in oxygen atmosphere," *Journal of Alloys and Compounds,* vol. 505, pp. 568-572, 2010.

[50]   R. Patel, P. Kumar, C. Prakash, and D. Agrawal, "Low temperature synthesis and dielectric, ferroelectric and piezoelectric study of microwave sintered BaTiO3 ceramics," *Ceramics International,* vol. 38, pp. 1585-1589, 2012.

[51]   Y.-F. Zhu, L. Zhang, T. Natsuki, Y.-Q. Fu, and Q.-Q. Ni, "Facile synthesis of BaTiO3 nanotubes and their microwave absorption properties," *ACS applied materials & interfaces,* vol. 4, pp. 2101-2106, 2012.

[52]   X. Zhao, W. Liu, W. Chen, and S. Li, "Preparation and properties of BaTiO3 ceramics from the fine ceramic powder," *Ceramics International,* vol. 41, pp. S111-S116, 2015.

[53]   G. Liu and J. E. Greedan, "Syntheses, structures, and characterization of 5-layer BaVO3-X (X= 0.2, 0.1, 0.0)," *Journal of Solid State Chemistry,* vol. 110, pp. 274-289, 1994.

[54]   Y. Oka, T. Yao, and N. Yamamoto, "Hydrothermal synthesis and crystal structure of BaV3O8," *Journal of Solid State Chemistry,* vol. 117, pp. 407-411, 1995.

[55]   P. Khatri, B. Behera, V. Srinivas, and R. Choudhary, "Structural and dielectric properties of Ba3V2O8 ceramics," *Current Applied Physics,* vol. 9, pp. 515-519, 2009.

[56]   J. Xu, C. Hu, Y. Xi, C. Peng, B. Wan, and X. He, "Synthesis, photoluminescence and magnetic properties of barium vanadate nanoflowers," *Materials Research Bulletin,* vol. 46, pp. 946-950, 2011.

[57]   K. Nishimura, I. Yamada, K. Oka, Y. Shimakawa, and M. Azuma, "High-pressure synthesis of BaVO3: A new cubic perovskite," *Journal of Physics and Chemistry of Solids,* vol. 75, pp. 710-712, 2014.

[58]   B. L. Chamberland, "Preparation and crystallographic properties of barium chromate (IV) polytypes," *Inorganic Chemistry,* vol. 8, pp. 286-290, 1969.

[59]   P. S. Haradem, B. L. Chamberland, and L. Katz, "The structure of the 27-layer polytype of BaCrO3," *Journal of Solid State Chemistry,* vol. 34, pp. 59-64, 1980.

[60]   B. Chamberland, "Crystal structure of the 4H BaCrO3 polytype," *Journal of Solid State Chemistry,* vol. 43, pp. 309-313, 1982.

[61]   B. Chamberland, "Crystal structure of the 6H BaCrO3 polytype," *Journal of Solid State Chemistry,* vol. 48, pp. 318-322, 1983.

[62]   A. M. Arevalo-Lopez, S. J. Reeves, and J. P. Attfield, "Ferrimagnetism in the High Pressure 6H-Perovskite BaCrO3," *Zeitschrift für anorganische und allgemeine Chemie,* vol. 640, pp. 2727-2729, 2014.

[63]   A. M. Arévalo-López and J. P. Attfield, "High-pressure BaCrO3 polytypes and the 5H–BaCrO2. 8 phase," *Journal of Solid State Chemistry,* vol. 232, pp. 236-240, 2015.

[64]   C. Hu, H. Liu, C. Lao, L. Zhang, D. Davidovic, and Z. Wang, "Size-manipulable synthesis of single-crystalline BaMnO3 and BaTi1/2Mn1/2O3 nanorods/nanowires," *The Journal of Physical Chemistry B,* vol. 110, pp. 14050-14054, 2006.

[65]   Y. Yang, Y. Jiang, Y. Wang, and Y. Sun, "Photoinduced decomposition of BaFeO3 during photodegradation of methyl orange," *Journal of Molecular Catalysis A: Chemical,* vol. 270, pp. 56-60, 2007.

[66]   N. Hayashi, T. Yamamoto, H. Kageyama, M. Nishi, Y. Watanabe, T. Kawakami*, et al.*, "BaFeO3: a ferromagnetic iron oxide," *Angewandte Chemie International Edition,* vol. 50, pp. 12547-12550, 2011.

[67]   V. Milt, M. Ulla, and E. Miro, "NOx trapping and soot combustion on BaCoO3 perovskite: LRS and FTIR characterization," *Applied Catalysis B: Environmental,* vol. 57, pp. 13-21, 2005.

[68]   Q. Shen, Y. Zheng, S. Li, H. Ding, Y. Xu, C. Zheng*, et al.*, "Optimize process parameters of microwave-assisted EDTA method using orthogonal experiment for novel BaCoO3-δ perovskite," *Journal of Alloys and Compounds,* vol. 658, pp. 125-131, 2016.

[69]   Y. Takeda, M. Shimada, F. Kanamaru, M. Koizumi, and N. Yamamoto, "Preparation and Magnetic Property of BaNiO3 Single Crystals," *Chemistry Letters,* vol. 3, pp. 107-108, 1974.

[70]   J. G. Lee, J. Hwang, H. J. Hwang, O. S. Jeon, J. Jang, O. Kwon*, et al.*, "A new family of perovskite catalysts for oxygen-evolution reaction in alkaline media: BaNiO3 and BaNi0. 83O2. 5," *Journal of the American Chemical Society,* vol. 138, pp. 3541-3547, 2016.

[71]   C. Krüger, W. Reichelt, U. Lubahn, H. Scheler, and H. Oppermann, "Synthesis of BaCuO2 by different ways," *Crystal Research and Technology,* vol. 26, pp. 701-707, 1991.

[72]   W. Mingmei, S. Qiang, H. Gang, R. Yufang, and W. Hongyiang, "Preparation and properties of BaCuO2. 5 and its related oxides," *Journal of Solid State Chemistry,* vol. 110, pp. 389-392, 1994.

[73]   U. Spitsbergen, "The crystal structures of BaZnO2, BaCoO2 and BaMnO2," *Acta Crystallographica,* vol. 13, pp. 197-198, 1960.

[74]   Y.-C. Chiang and K.-S. Chang, "Fabrication of Ba1– xZnO2 nanowires using solvothermal synthesis: Piezotronic and piezophototronic performance characterization," *Applied Surface Science,* vol. 445, pp. 71-76, 2018.

[75]   J. Hombo, Y. Matsumoto, and T. Kawano, "Electrical conductivities of SrFeO3δ and BaFeO3− δ perovskites," *Journal of Solid State Chemistry,* vol. 84, pp. 138-143, 1990.

[76]   I. Halasz, V. Fulop, I. Kirschner, and T. Porjesz, "Thermoanalytical and x-ray diffraction investigations of Ba2Cu3O5+ d for preparation of Y-Ba-Cu-O superconductors," *Journal of crystal growth,* vol. 91, pp. 444-449, 1988.

[77]   T. Kopte and E. Hegenbarth, "Thermal Conductivity of BaCuO2+ x at Low Temperatures and High Magnetic Fields," *physica status solidi (b),* vol. 156, 1989.

[78]   A. Maiorova, S. Mudretsova, M. Kovba, A. Monaenkova, and A. Popova, "Thermochemical characteristics of nonstoichiometric Ba2Cu3O5: II. Thermal transformations," *Physica C: Superconductivity,* vol. 218, pp. 137-140, 1993.

[79]   N. Topnani, S. Kushwaha, and T. Athar, "Wet synthesis of copper oxide nanopowder," *International Journal of Green Nanotechnology: Materials Science & Engineering,* vol. 1, pp. M67-M73, 2010.

[80]   V. Bannikov, "Elastic, electronic and magnetic properties of new oxide perovskite BaVO3: A first-principles study," *Materials Chemistry and Physics,* vol. 171, pp. 119-125, 2016.

[81]   C. Karagiozov and D. Momchilova, "Synthesis of nano-sized particles from metal carbonates by the method of reversed mycelles," *Chemical Engineering and Processing: Process Intensification,* vol. 44, pp. 115-119, 2005.

[82]   Y. Ni, H. Zhang, J. Hong, L. Zhang, and X. Wei, "PAM-directed fabrication, shape evolution and formation mechanism of BaCO3 crystals with higher-order superstructures," *Journal of Crystal Growth,* vol. 310, pp. 4460-4467, 2008.

[83]   Q. Zhang, C. Chen, and L. Fang, "Synthesis of thorny BaCO3 dendritic structures via a simple PEG-assisted method," *Materials Chemistry and Physics,* vol. 111, pp. 191-194, 2008.

[84]   S. Lv, J. Sheng, S. Zhang, and W. Sun, "Effects of reaction time and citric acid contents on the morphologies of BaCO3 via PVP-assisted method," *Materials Research Bulletin,* vol. 43, pp. 1099-1105, 2008.

[85]   A. Omrani, A. A. Rostami, and E. Sedaghat, "Kinetics of cure for a coating system including DGEBA (n= 0)/1, 8-NDA and barium carbonate," *Thermochimica Acta,* vol. 497, pp. 21-26, 2010.

[86]   T. Hong, F. Chen, and C. Xia, "Barium carbonate nanoparticle to enhance oxygen reduction activity of strontium doped lanthanum ferrite for solid oxide fuel cell," *Journal of Power Sources,* vol. 278, pp. 741-750, 2015.

[87]   P. Nagajyothi, M. Pandurangan, T. Sreekanth, and J. Shim, "In vitro anticancer potential of BaCO3 nanoparticles synthesized via green route," *Journal of Photochemistry and Photobiology B: Biology,* vol. 156, pp. 29-34, 2016.

[88]   P. Hlabela, J. Maree, and D. Bruinsma, "Barium carbonate process for sulphate and metal removal from mine water," *Mine Water and the Environment,* vol. 26, pp. 14-22, 2007.

[89]   H. Zhang, C. Hu, M. Zhang, R. Yang, and C. Zheng, "Synthesis of BaCO3 Nanowires and Their Humidity Sensitive Property," *Journal of nanoscience and nanotechnology,* vol. 11, pp. 10706-10709, 2011.

[90]   X. Wu, L. Wang, F. Luo, B. Ma, C. Zhan, and Y. Qiu, "BaCO3 modification of TiO2 electrodes in quasi-solid-state dye-sensitized solar cells: performance improvement and possible mechanism," *The Journal of Physical Chemistry C,* vol. 111, pp. 8075-8079, 2007.

[91]   E. Brzozowski, J. Sanchez, and M. Castro, "BaCo 3–TiO 2 solid state reaction: A kinetic study," *Journal of Materials Synthesis and Processing,* vol. 10, pp. 1-5, 2002.

[92]   S. More and R. Topare, "The review of various synthesis methods of barium titanate with the enhanced dielectric properties," in *AIP Conference Proceedings*, 2016, p. 020560.

[93]   V. Pavlović, B. Stojanović, V. Pavlović, Z. Marinković-Stanojević, L. Živković, and M. Ristić, "Synthesis of BaTiO3 from a mechanically activated BaCO3-TiO2 system," *Science of Sintering,* vol. 40, pp. 21-26, 2008.

[94]   H. H. Singh, A. D. Sharma, and H. B. Sharma, "Dielectric And Electrical Properties Of Barium Zirconate Titanate Ceramics," *International Journal of Engineering Technology, Management and Applied Sciences,* vol. 5, pp. 178-184, 2017.

[95]   K. Oksuz, S. Sen, and U. Sen, "Influence of ZrO2 Addition on the Structure and Dielectric Properties of BaTiO3 Ceramics," *Acta Physica Polonica, A.,* vol. 131, 2017.

[96]   H. Z. Akbas, Z. Aydin, O. Yilmaz, and S. Turgut, "Effects of ultrasonication and conventional mechanical homogenization processes on the structures and dielectric properties of BaTiO3 ceramics," *Ultrasonics sonochemistry,* vol. 34, pp. 873-880, 2017.

[97]   M. El-Mansy, N. Shash, M. Maklad, and E. Diefallah, "Effect of growing barium ferrite phases on the electrical conduction in Fe2O3/BaCo3 composite," *Materials chemistry and physics,* vol. 52, pp. 71-77, 1998.

[98]   S. Capraro, J.-P. Chatelon, M. Le Berre, H. Joisten, T. Rouiller, B. Bayard*, et al.*, "Barium ferrite thick films for microwave applications," *Journal of Magnetism and Magnetic Materials,* vol. 272, pp. E1805-E1806, 2004.

[99]   W. Widanarto, M. Jandra, S. Ghoshal, M. Effendi, and W. Cahyanto, "BaCO3 mediated modifications in structural and magnetic properties of natural nanoferrites," *Journal of Physics and Chemistry of Solids,* vol. 79, pp. 78-81, 2015.

[100]   Q. He, H. Wang, G. Wen, Y. Sun, and B. Yao, "Formation and properties of BaxFe3– xO4 with spinel structure by mechanochemical reaction of α-Fe2O3 and BaCO3," *Journal of Alloys and Compounds,* vol. 486, pp. 246-249, 2009.

[101]   F. Zhang, X. Wang, X. Zhang, M. Tursun, and H. Yu, "Promotion by Co of a NiO-BaCO3 catalyst for N2O decomposition," *Chinese Journal of Catalysis,* vol. 36, pp. 344-347, 2015.

[102]   A. K. Zak, A. M. Hashim, and M. Darroudi, "Optical properties of ZnO/BaCO 3 nanocomposites in UV and visible regions," *Nanoscale research letters,* vol. 9, p. 399, 2014.

[103]   V. A. Gasparov, S. Ermolov, G. Strukova, N. Sidorov, S. Khassanov, H.-S. Wang*, et al.*, "Superconducting and anomalous electron transport properties and electronic structure of BaNbO 3– x and Ba 2 Nb 5 O x films," *Physical Review B,* vol. 63, p. 174512, 2001.

[104]   G. Strukova, V. Kedrov, V. Zverev, S. Khasanov, I. Ovchinnikov, I. Batov*, et al.*, "On the synthesis and the electric and magnetic properties of superconducting barium– niobium–oxide compounds," *Physica C: Superconductivity,* vol. 291, pp. 207-212, 1997.

[105]   H. Y. He, "Structural and Magnetic Property-xNfxFe2O4 Nanoparticles Synthesized by Hydrothermal Method," *International Journal of Applied Ceramic Technology,* vol. 11, pp. 626-636, 2014.

[106]   J. Chocha, "Synthesis and Characteristics of Different Compositions of Nd1-xBaxMnO3 Nano-crystalline Perovskite."

[107]   T. Roisnel and J. Rodríquez-Carvajal, "WinPLOTR: a windows tool for powder diffraction pattern analysis," in *Materials Science Forum*, 2001, pp. 118-123.

[108]   I. Gul and A. Maqsood, "Structural, magnetic and electrical properties of cobalt ferrites prepared by the sol–gel route," *Journal of Alloys and Compounds,* vol. 465, pp. 227-231, 2008.

[109]   J. K. Rao, A. Raizada, D. Ganguly, M. M. Mankad, S. Satayanarayana, and G. Madhu, "Investigation of structural and electrical properties of novel CuO–PVA nanocomposite films," *Journal of materials science,* vol. 50, pp. 7064-7074, 2015.

[110]   A. Azam, A. S. Ahmed, M. S. Ansari, and A. H. Naqvi, "Study of electrical properties of nickel doped SnO 2 ceramic nanoparticles," *Journal of Alloys and Compounds,* vol. 506, pp. 237-242, 2010.

[111]   H. El-Mallah, "AC electrical conductivity and dielectric properties of perovskite (Pb, Ca) TiO3 ceramic," *Acta Physica Polonica-Series A General Physics,* vol. 122, p. 174, 2012.

[112]   M. Nevriva, E. Pollert, and J. Sestak, "High-temperature DTA of ceramic superconductor YBa sub 2 Cu sub 3 O sub 7 sub- sub y," *Thermochimica acta,* vol. 127, pp. 395-7, 1988.

[113]   D. De Leeuw, C. Mutsaers, C. Langereis, H. Smoorenburg, and P. Rommers, "Compounds and phase compatibilities in the system Y2O3-BaO-CuO at 950° C," *Physica C: Superconductivity,* vol. 152, pp. 39-49, 1988.

[114]   L. Klinkova, V. Nikolaichik, N. Barkovskii, and V. Fedotov, "New phases in the barium-rich region of the BaO-BaCuO 2 system," *Bulletin of the Russian Academy of Sciences: Physics,* vol. 73, pp. 1104-1106, 2009.

[115]   L. Klinkova, I. Sojkina, I. Zver'kova, S. Zver'kov, S. Shevchenko, and N. Ganovich, "Phase equilibria in Y-Ba-Cu-O system in the region of YBa 2 Cu 3 O x," *Izvestiya Akademii Nauk SSSR, Neorganicheskie Materialy,* vol. 25, pp. 2037-2041, 1989.

[116]   T. Lindemer and E. Specht, "The BaO ⋅ Cu ⋅ CuO system. Solid-liquid equilibria and thermodynamics of BaCuO2 and BaCu2O2," *Physica C: Superconductivity,* vol. 255, pp. 81-94, 1995.

[117]   W. Zhang, K. Osamura, and S. Ochiai, "Phase Diagram of the BaO-CuO Binary System," *Journal of the American Ceramic Society,* vol. 73, pp. 1958-1964, 1990.